Numerical Simulation of Orion CEV re-entry vehicle

Patel Rakeshkumar K.

A Thesis Submitted to

Indian Institute of Technology Hyderabad

In Partial Fulfillment of the Requirements for

The Degree of Master of Technology

Department of Mechanical Engineering

July 2013

Declaration

I declare that this written submission represents my ideas in my own words, and where ideas or words of others have been included, I have adequately cited and referenced the original sources. I also declare that I have adhered to all principles of academic honesty and integrity and have not misrepresented or fabricated or falsified any idea/data/fact/source in my submission. I understand that any violation of the above will be a cause for disciplinary action by the Institute and can also evoke penal action from the sources that have thus not been properly cited, or from whom proper permission has not been taken when needed.

(Signature)

(Patel Rakeshkumar K.)

(ME11M13)

Approval Sheet

This Thesis entitled **Numerical Simulation of Orion CEV re-entry vehicle** by Patel Rakeshkumar K. is approved for the degree of Master of Technology from IIT Hyderabad

(Dr. K. Arul Prakash) External Examiner
Department of Applied Mechanics
IIT Madras

(Dr. Raja Banerjee) Internal Examiner
Department of Mechanical Engineering
IIT Hyderabad

(Dr. K.Venktasubbaiah) Adviser
Department of Mechanical Engineering
IIT Hyderabad

(Dr. Narasimha Mangadoddy) Chairman
Department of Chemical Engineering
IIT Hyderabad

Acknowledgements

The work presented here would not have been possible without the guidance and help of many people who in one way or the other extended their valuable assistance. I take this opportunity to express my sincere thanks towards them.

First and foremost, I would like to thank my advisor Dr.K.Venkatasubbiah for his phenomenal guidance and support. I am deeply grateful for his valuable mentoring and supervision during the course of this thesis work. I have learnt so much in the countless hours of discussions we had in which he has patiently explained all the intricate concepts in a simple manner. Apart from the technical inputs, Im also thankful for his moral support in my life and career.

I would like to express my thanks to Prof.Vinayak Eswaran, Dr.Raja Banarjee, Dr. Bhaskar Kumur, Dr. Ravikiran Sangras and Dr. Ashok Pandey who taught me many fundamental of subjects during my stay at IIT Hyderabad.

I am thankful to my friends in Thermofluid family especially Nikhil Kalkote, Mudassar Sheikh, Pasham Nithish Reddy, Pankaj Kumar, Amit Bhagel and Santosh kumar for being there with me at all times. I sincerely acknowledge their encouragement and assistance that I received during the course of our master's program.

I am very much grateful to Mr. Madhu for installation of many software and teach many computation processes. I am thankful to Mr.Srikanth and Ms.Nagalakshmi for being on my side and providing valuable support during my thesis work. I am very thankful to Phd scholars Harish, Rajesh and Saritha for their valuable inputs. I am also grateful to my Vatsalya, Varun , Ashwini, shashi , Anil, Girish, Chhabikant who have helped me to expand my knowledge. I am very thankful to my roommates Ramesh and Sanjeev for enjoyable life with them. I am also thankful to entire M tech Boys hostel series family for pleasant and joyful life at IIT Hyderabad.

Finally, I thank my family for all the constant love and support I received throughout the years. I am thankful to God for providing me with all the resources and showing me the right path.

Dedicated to my loving Family and Nation....

Abstract

Aerothermodynamics analysis of Orion Crew Exploration Vehicle (CEV) re-entry vehicle at high altitude and low altitude has been studied numerically. At high altitude in the rarefied flow regime non-continuum technique such as Direct Simulation Monte Carlo (DSMC) method is used to solve the Boltzmann equation of kinetic theory. Results are reported at different altitudes in the rarefied regime for ideal gas and real gas model. The effects of nose radius and free stream velocity are presented. The estimation of bow shock strength and peak heat flux is higher for ideal gas compared to real gas model. The flow field characteristics have shown significant change with increase in free stream velocity. The Reynolds averaged Navier-stokes methods along with sparart-Allmaras turbulent model are used to compute flow field in high density region at low altitude. Effect of the free stream velocity and altitude at high density on flow field and heat flux generation on surface of re-entry vehicle studied. Present results are matching very well with the experimental results available from the literature for both regime.

Contents

List of Figures

.

List of Tables

.

Nomenclature

R_n	Nose radius
R	Base radius
K_n	Knudsen number
λ	Mean free path
L	Characteristic length
f	Velocity distribution function
u,v,w	Velocity Components in Cartesian coordinate system
δ	Molecular spacing
c	Resultant velocity
F	Force per unit mass
n	Number density
c_r	Relative velocity
σ	Cross section area
Ω	Solid angle
mcs	Mean collision separation
n	Temperature exponent
K	Boltzmann constant = 38×10^{-23}J/K
Ea	Activation energy
k_f	Forward reaction rate
k_r	Reverse reaction rate
C_f	Pre-exponential factor in the forward rate equation
C_r	Pre-exponential factor in the reverse rate equation
U	Velocity
T	Temperature
ρ	Density
M	Mach number
P	Pressure
T_w	Wall temperature
C_p	Pressure Coefficient
S_t	Stanton number
L	Reference length =0.1 m (in chapter 3)
H	Altitude
Re	Reynolds number
H_0	Total enthalpy
H	Enthalpy
q	Surface heat flux

D	Diameter of Re-entry vehicle
μ	Viscosity
w	wall
∞	Free stream condition
f	Forward reaction
r	Reverse reaction

Chapter 1

Introduction

One of the notable research in aerospace engineering field is human space exploration. Current Space exploration includes manned and unmanned program missions to investigate on planets like mars, moon and outer space through International Space Station (ISS). Mars missions objective is to conduct a research on fundamental science such as astrology and geology. Renewed an ambition to send men to moon since earlier missions created questions such as the presence of water ice in the permanently shadowed craters near the lunar poles and possibility of livable life. So there is new fundamental science to be performed. ISS is joint venture of five international space agencies of America, Canada, Japan, Russia and Europe. Space agencies are conducting research in ISS such as effect of micro gravity, microbial vaccine development, monitoring and forecasting of weather and atmosphere.

1.1 Re-entry vehicle

Successfully to complete the space exploration mission this required a considerable amount of energy to go beyond the gravity of earth to enter the orbit. Lot of challenges and difficulties have to face while returning from orbit. All of the energy used to get into the orbit that has to dissipate on the way back to earth in the form of extreme heat energy according to the conservation of energy principle. In addition to heat energy there is an aerodynamic concern of the vehicle since the speed of the vehicle is very high. Object or vehicle used to deliver people or payload safely through atmosphere of the planet (earth in case of returning) is called re-entry vehicle. Ballistic entry of missile through earth atmosphere is also come under the re- entry vehicle. Successfully re -entry of vehicle under high heat flux situation this requires a proper thermal protection system (TPC).

1.1.1 Thermal protection system

In a broad sense, there are three thermal protection systems: passive, semi-passive and active. Any type of thermal protection system depends on magnitude and duration of heat load on the vehicle and operating conditions of the vehicle.

Passive thermal protection systems have no moving parts. They are simple but have less capability. These concepts have fallen into three general categories: heat sink, hot structure and insulated structure. The heat sink absorbs almost all of the incident heat and stores it in a large usually metallic mass. This concept limited to short heat pulses. A hot structure allows the temperature to rise until the heat being radiated from the surface is equal to the incident heating, much like heating element of an electric stove. This concept is limited by the surface temperature of the structural material. The Inconel X hot structure of the X-15 plane could with stand up to about 922 K which is the maximum temperature for this concept. Insulated structures use an outer shell that radiates most incident heat away from an underlying structure protects by some insulating material, generally high temperature ceramic-fiber batt insulation. Both the magnitude and duration of the heat pulse are upper limit for use of insulated systems.

There are two semi passive concepts: Heat pipes and ablation. Heat pipes are attractive where there is a localized area of high heating with an adjacent area of low heating. Ablation is a process in which a material (ablator) sacrifices itself to protect the underlying structure. These ablative materials may be chemically constructed (usually some form of fiberglass or a spray-on resin-based coating) or made from natural materials (both the Chinese and Soviets/Russians used oak wood on some early reentry vehicles). As heat is absorbed by the ablator, part of the material decomposes into a gas, which carries heat away from the surface. Near the surface, exposure to higher temperatures causes more complete pyrolysis, thus the surface shows a more complete decomposition than the inner layers and forms a char, much like charcoal. The vaporization of an ablator is an endothermic reaction i.e., it needs energy input to proceed. A proper ablator will absorb the heat flux incident to its surface and vaporize at a rate proportional to the magnitude of the heat flux. The heat is carried away with the vaporized material.

Third concept is active cooling system in which coolant ejected from the vehicle surface blocks most of the heat from reaching the underlying structure. These concepts use a pump to bring liquid coolant from a remote reservoir on to the surface of the vehicle. Sometime circulation of coolant (water or liquid metal) used around the hot area by cooling through a heat exchanger or radiator. The coolant, pump and radiator systems added considerable weight therefore third concept is not truly practicable.

The design phase of thermal protection system requires accurate predication of the surface quantities. These quantities are typically are heat flux, pressure, temperature and shear stress. Peak heat flux and pressure selects the TPS material. Heat flux selects the thickness of the TPS material stack. As computer architect becomes advanced, numerical computation methods play an important role for predication of this surface quantities.

1.1.2 History of Re-entry vehicle

During the world war II, In 1943 Under the guidance of Wernher von braun(a German scientists and one of the leader in the development of rocket technology) Germany initiated the development of short range ballistic missiles. They had a working vehicle called Assembly-4(A4). After successful experiments in 1944, the A4 reached an altitude of only 50 to 60 miles(80.47 to 96.56 kms) after which it descended in a ballistic trajectory with a maximum velocity approximately Mach 4 and range of 200 miles(321.89 kms). The temperatures it experienced while streaking through the thick atmosphere near Earth's surface were well within the heat and strength capability of conventional steel and aluminum alloys [1].

In 1953, same team of A4 was made missiles that flew very high altitude and far away than A4 but it carried much larger payload and reached a maximum velocity of Mach 5.5 during re-entry. Improved versions, called Jupiter that were developed few year later extended the maximum range to 1500 miles(2414 kms) and reached Mach 15 during re-entry from a 390 mile(627.44 km) peak altitude. Under X plane series of experimental aircraft X-15 aircraft designed and it encompasses 199 fights between June 1959 and October 1968. By July 1962, X-15 had flown more than Mach 6 and above 30000 feet. X-15 project testing provided valuable data which used in aircraft and spacecraft design. As of now,the X-15 holds the official world record for the fastest speed ever reached by a manned aircraft. Its maximum speed was 4,520 miles per hour (7,274 km/h) [2].

In August 1958, President of US Eisenhower signed the National Aeronautic and space act of 1958 and assigned the nation's human space flight mission to NASA. After this assignment NASA started project Mercury and it run from 1959 to 1963 with two goals: send the human in orbit around the earth and also should be done before the Soviet Union. They have succeeded on May 1961, Alan Shepard became the first American in space. Re-entry vehicle shape used in the mercury project was blunt shape capsules based on blunt body aerodynamics. The spacecraft was designed with TPS material either a beryllium or ablative fiberglass heat shield to protect the aerodynamic heating during on reentry. After re-entry, parachute was deployed to safely landing on the sea water [3].

On the same year 12 April 1961, The Vostok spacecraft of Union Soviet Union put Yuri Gagarin in outer orbit and became first person to travel in space. Re-entry vehicle shape of the Vostok was spherical and it required the thermal protection from all side.

Figure 1.1: vostok re-entry module

Project Gemini was the second human spaceflight program of NASA and it was modified version of project mercury. It performed ten manned flights occurring in 1965 and 1966. Project Gemini was made to put two-man in space followed by one in Mercury [4].

Project Apollo started with US President John F. Kennedy's national goal of "landing a man on the Moon and returning him safely to the Earth " in 1968. Apollo space craft designs were extension of Mercury and Gemini project with capacity of three astronauts. Re-entry capsule shape was same as Gemini project of blunt shape and thermal protection system based on ablation process using Avcoat, a glass filled epoxy-novalc system. On July 20, 1969 Apollo 11 successfully accomplished Kennedy's goal when astronauts Neil Armstrong and Buzz Aldrin landed on lunar surface. In between 1968 to 1972 six Apollo spaceflights were done and 12 men walked on the Moon [5].

Apollo module were further used for three missions of Skylab, United states first space station between 1973 to 1974 and re-entry on earth in 1979. After that other space laboratory started by NASA in 1983 and 22 shuttle missions were done from 1983 to 1988. Russia built space station Mir in between 1986 to 1996 and Soyus, a modified version of Vostok used as primary re-entry vehicle and after that Mir shuttle used as re-entry vehicle.

Figure 1.2: apollo re-entry vehicle

Internation Space Station(ISS) work started as joint venture of five space agency in 1998. Russian space craft Soyuz and Progress space craft , European Space Agency(ESA) unmanned space craft named Automated Transfer vehicle(ATV), Japaneses unmanned space craft H-II Transfer Vehicle used for delivery of man and payload to ISS. Orion, a NASA next generation space craft will also serve mission to ISS.

Space shuttle type re-entry vehicle with wings are easy landing on run ways as plane and also reusable but their use limited up to lower orbit of earth. Space shuttle are designed only up to 17500 mph(28163.52 km/h) speed but for go out of outer lower orbit of earth it should required speed more than 17500 mph(28163.52 km/h) to go outside of the earth gravitation. Entering the Earth's atmosphere at this high speed would destroy the shuttle because it would exceed the wing and fuselage load limits. Currently, there is no thermal protection system that would protect the wings from such a high heat load. The space craft is preferred than space shuttle to enter the orbit due to more load capacity, higher speed and better thermal protection system.

The Indian manned spacecraft temporarily named Orbital Vehicle is intended to be the basis of the indigenous Indian human spaceflight program by ISRO. The capsule will be designed to carry three people, and a planned upgraded version will be equipped with rendezvous and docking capability However the future of the project is in doubt due to funding problems and numerous technical challenges faced.

Country	Agency	vehicle	Mission
United states	National Aeronautics and Space Administration(NASA)	Orion	Mars,Moon ISS
Russia	Russian Federal Space Agency	Soyuz	ISS
Europe	European Space Agency(ESA)	Automatic Transfer Vehicle (ATV)	ISS
Japan	Japan Aerospace Exploration Agency(JAXA)	H-II Transfer Vehicle(HTV)	ISS unmanned
China	China National Space Administration(CNSA)	Shenzhou	
India	Indian Space Research Organization (ISRO)	Orbiatl Vehicle(OV)	

Table 1.1: Current Re-entry vehicle

1.1.3 Orion CEV

The Project Orion Crew Exploration Vehicle (CEV) was defined by NASA's Exploration Systems Architecture study in 2005 for NASA's next manned space vehicle [6]. The CEV will support NASA's exploration missions by providing crew access to the International Space Station, the moon, and Mars. Journey of Space shuttle with Orion CEV takes place in 2014 as per NASA plan. The geometry of Orion CEV is similar to that of Apollo but larger in size and mass is almost double of Apollo. The Orion Crew Module will hold four to six crew members, depending on the type of mission: the LEO version will be able to carry six crew members to the International Space Station, while the lunar and Mars versions would carry a crew of four and six members respectively. Although it may have an Apollo shape, the new spacecraft will have significant advances including:

- The safest most efficient shape for going beyond low Earth orbit
- Advanced materials, avionics and manufacturing process.

Figure 1.3: Orion spacecraft

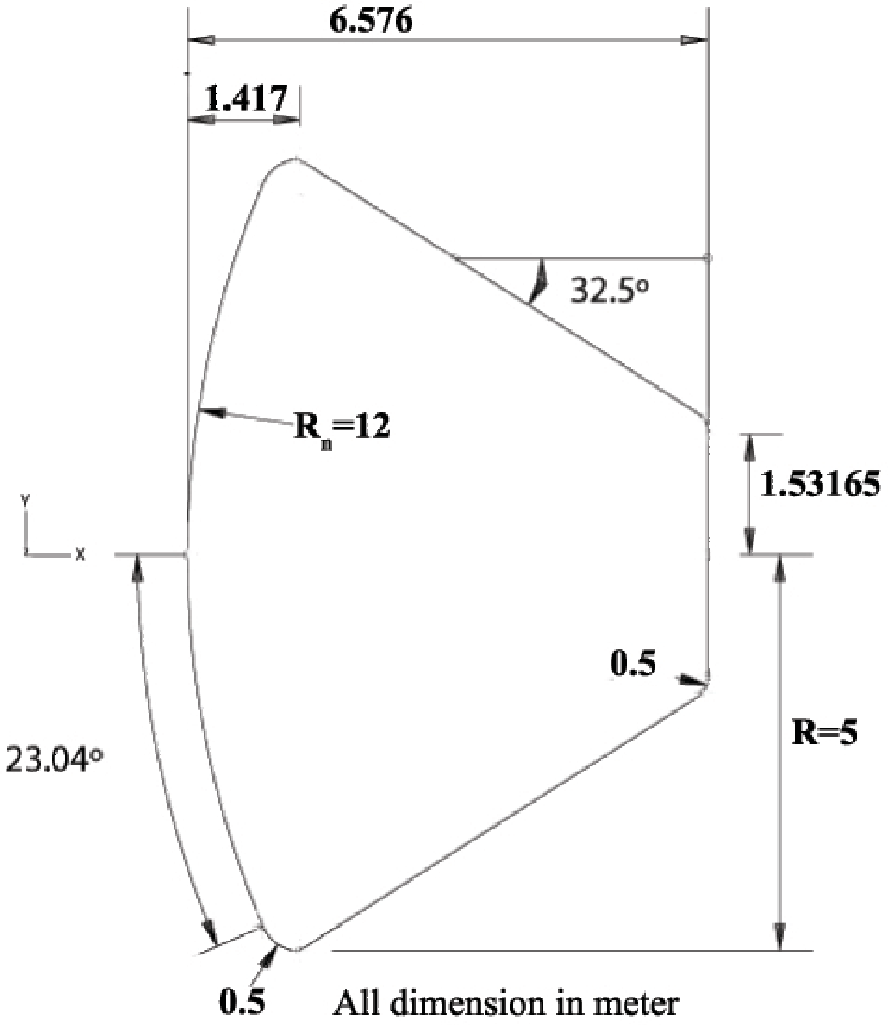

Figure 1.4: Schematic diagram of Orion CEV.

- Computers and the experience gained from 40 years of human space flight
- Increased volume. It can carry more crew and cargo.
- Improved operational efficiency and overall capability in a vehicle shaped much like the original Apollo capsule

Heat load during the orion re-entry is very high therefore thermal protection system of Orion will done by semi passive ablation process. Avcoat and PICA(Phenolic Impregnated Carbon Ablator) will be used as ablator for Orion CEV heat shied. Recovery of Orion CEV will done by landing on sea water with help of parachutes .

1.2 Literature Survey

Re-entry vehicle enters the earth atmosphere at very high speed and these leads to formation of bow shock in front of the vehicle and also increase the aerodynamic heating of the body. The design of re-entry vehicles requires accurate predictions of the surface quantities. These quantities are typically the heat flux, pressure and shear stress, from which the aerodynamic forces and moments can be calculated. These variables govern not only the aerodynamic performance of the vehicle, but also determine the selection and sizing of the thermal protection system (TPS), which protects the vehicle from the extreme temperatures encountered at high velocities. Unfortunately, it is very difficult and expensive to reproduce in ground based experiments and flight tests the conditions met from a vehicle during re-entry. For this reason, computational methods have played a prominent role in aerodynamics of re-entry vehicle.

In the literature blunt shape of re-entry vehicle was proposed by Allen [7] and Eggers [8] and their work in the history considered as pioneer work in the field of hypersonic flows. They pointed out that the blunt shape was optimum for relatively light weight reentry bodies.

History of hypersonic flow were given by Heppenheimer [9] . Moretti and Abbetti [10] numerically studied the supersonic flow over blunt body. Bertin and Cummings [11] reported the progress of research in the field of hypesonic flows in the last fifty years. Recently, Hollis and Borrelli [12] reported the review article on aerothermodynamics of blunt body entry vehicles.

Computational flow field analysis of blunt body re-entry vehicle was reported by viviani [13]. He has solved the Euler and Navier-stokes equations with the assumption of low earth orbit re-entry scenario. Pezzella [14] reported the aerodynamic and aerothermodynamic trade-off analysis for configuration design of re-entry vehicle. Stella *et al.* [15] reported the flow field around YES-2 re-entry capsule using CFD. They have used a simplified model based on modified specific heats to account the dissociate effects. Pezzella [16] have studied the hypersonic environment assessment of the FTB-X re-entry vehicle. He has considered the air as a perfect gas model and analyses are based on laminar flow conditions. Ohtake [17] have studied the thermal analysis of thermal protection system for the re-entry vehicle. He has performed flow and structure analysis using Finite element methods. Savino *et al.* [18] studied the thermal analysis of thermal protection system for the re-entry vehicle. They have investigated the thermal response of ultra-high temperature ceramics (UHTC) material for thermal protection system of re-entry vehicle.

A hypersonic vehicle, entering an atmosphere, will go through many different flow regimes due to the change in atmospheric density with altitude. At lower altitudes where the

density is high and the Knudsen number is low, flows should be simulated using traditional computational fluid dynamics (CFD) techniques by numerically solving the Navier-Stokes equations. However, when the Knudsen number becomes larger, the continuum assumption in the Navier-Stokes equations starts to breakdown. At higher altitudes, in the rarefied flow regime, only a non-continuum technique can be used, such as the classical Direct Simulation Monte Carlo (DSMC) method that is particle method for simulating non-equilibrium gas flows.

Bird[19] have developed DS2V code based on DSMC methods to solve rarefied low density flow regime. DS2V software would be very useful to analyze flow field over a re-entry vehicle at high altitude because it includes the chemical reaction, dissociation and ionization phenomena′ s which are not possible in many of conventional fluid flow solvers. Survey and review of Boltzmann equation methods for rarefied gas dynamic flows were given by Bellomo *et al.* [20]. Comparisons of rarefied flow predictions with experimental data were reported for Mars Rovers Vehicles (MSL)in [21] [25]. Vota *et al.* [26] studied the hypersonic high altitude aerothermodynamics of a space re-entry vehicle. They have investigated the rarefaction effects in the prediction of aero thermal loads of re-entry vehicle.

In the work Kruse *et al.* [22] a considerable amount of effort devoted to identify laminar and turbulent regions in the flow around the Apollo shaped body. Hollis et al. [23] did experiments to predicate turbulent aero heating over a Orion CEV scaled model with high density perfect nitrogen gas and compared results with LAURA code. Hypersonic turbulent flow simulations over FIRE II re-entry vehicle done by sinhaet al. [24] by use of sparart-Allmaras turbulent model.

1.3 Motivation

Orion CEV is future human space exploration vehicle and it is in design phase. Very few numerical studies on Orion CEV re-entry vehicle at high altitude were reported earlier. The present investigation has been motivated for the following points. (i) Detailed analysis of aerothermodynamics of Orion CEV re-entry vehicle at high and low altitudes for different velocities are not available in the literature. (ii) Effect of nose radius on aerodynamic heating are not exist.

1.4 Objective of the Present work

The main objective of present work is to study the flow field characteristics and estimation of maximum heat flux around Orion CEV re-entry vehicle in rarefied regime at high altitude and high density regime at low altitude.

- Effect of altitude
- Effect of free stream velocity
- Effect of nose radius

1.5 Outline of the thesis

- Chapter 2 gives the description about the governing equations and numerical method for high and low density region.
- Chapter 3 deals with validation and results and discussion in low density region
- Chapter 4 deals with grid independency test, validation and results and discussion in high density region.
- Chapter 5 and 6 Conclusion and Scope of Future work.

Chapter 2

Formulation and Numerical Methods

Re-entry vehicle return to earth will go through different flow regimes due to change in atmospheric density with altitude. In gas dynamics studies, the basic criteria of the flow regime is the Knudsen number:

$$K_n = \frac{\lambda}{L} \tag{2.1}$$

where λ is the mean free path and L is a characteristic length of flow field. The flow-regime is continuum when a Knudsen number tends to zero. While studying the gas flow in this regime, one can disregard its microscopic structure and consider only its macro parameters such as density, velocity or temperature. For a Knudsen number tending to infinity the flow regime can be considered as free-molecular. In this case, particle collisions with the body surface play the determining role.

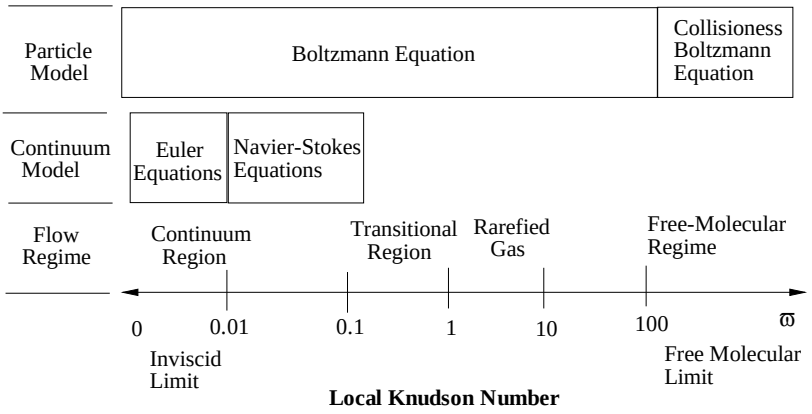

Figure 2.1: The Knudsen number limits for each method[27]

There is a transitional regime between the free-molecular and continuum regimes, where not only gas-surface collisions but also inter molecular collisions are important. Free-molecular and transitional regimes are the subject of Rarefied Gas Dynamics. Besides viscosity and other important viscous effects (including heat conduction, relaxation, diffusion, and irreversible chemical reactions), strong thermal non-equilibrium of the flow is an important feature of rarefied hypersonic flows.

A Re-entry vehicle, entering an atmosphere, will go through many different flow regimes due to the change in atmospheric density with altitude. These regimes are characterized by Knudsen number as shown in Fig. 2.1. This figure gives four regimes and indicate the governing equations that are accurate for each regime.

2.1 Formulation in low density region

2.1.1 Governing equations

At high altitude (around above 92 km) density of air is very low and flow region is rarefied in nature. From Fig. 2.1 it is noticed that in rarefied gas region continuum flow equations of Euler and Navier-Stokes may not be valid. In the rarefied regime the governing equation is the Boltzmann equation of kinetic theory [28].

Boltzmann equation

The Boltzmann equation states a relationship between the velocity distribution function f and the variables velocity V, space position vector r and time t. This equation, derived in 1872, is a more operative version of the Liouville equation. The Liouville equation is written in terms of probability density while the Boltzmann equation is written in terms of velocity distribution function.
velocity distribution function f is defined as

$$dn = nf(c)dudvdw \tag{2.2}$$

where dn is the number of molecules in the sample with velocity components u to u+du, v to v+dv,and w to w+dw. The product du dv dw may be identified as a volume element in velocity space and is denoted by dc.

The Boltzmann equation relies on the following hypotheses:

1. Gas is dilute. By definition, a gas is dilute if the molecular spacing δ ($\delta = n^{-1/3}$) is much greater than the molecular diameter (d): $\delta/d >> 1$. This hypothesis implies that the collisions are only bi-molecular and involve only weak inter molecular forces.

2. Inter molecular collisions are perfectly elastic. A collision is elastic if: there is no exchange of energy between transnational degree of freedom (kinetic energy) and rotational and vibration degrees of freedom (internal energy).

3. "Molecular chaos". This hypothesis relies on the concept of stochastic independence, the distribution function of a generic molecule is independent of the distribution function of other molecules.

Boltzmann equation is made of four terms, providing the change in molecules in the phase space by three ways: (i)The convection of molecules across the face of dr by the molecule velocity c. (ii) The convection of molecule across the surface of dc as a result of the external force per unit mass F. (iii) The scattering of molecules into and out of dc dr as a result of inter molecules collisions. The unknown distribution function f is both in derivative and in integral, therefore the Boltzmann equation is an integral-differential equation. Its solution presents overwhelming theoretical and numerical difficulties. A mixture of gases, made up by s spices, required a distribution function, different for each spices. In this case, The Boltzmann equation becomes a system of s independent equations. where p and q represent particular spices.

$$\frac{\partial}{\partial t}(n_p f_p) + c_p \frac{\partial}{\partial r}(n_p f_p) + F \frac{\partial}{\partial c}(n_p f_p) = \sum_{q=1}^{s} \int_{-\infty}^{+\infty} \int_{0}^{4\pi} n_p n_q ({f_p}^* {f_{1q}}^* - f_p f_{1q}) c_{rpq} \sigma_{pq} d\Omega dc_{1q} \tag{2.3}$$

where n is number density, f is velocity distribution function, c is resultant velocity, f without and with 1 shows first and second molecules respectively. f Without * means pre collision and * means post collision of molecule. F is the external force per unit mass. c_r is the relative velocity before collision.σ is the cross section area of molecules. Ω is solid angle.

Now a days, the solution of Boltzmann equation relays on molecular methods such as Molecular Dynamics and specially Direct Simulation Monte Carlo (DSMC). Both Molecular dynamics and DSMC method are numerical computational method. Molecular dynamics method is deterministic in nature while DSMC is statistic. In fact number of molecules in Molecular Dynamics is the same like the number of the real molecules that requires large number information of each molecule to store and large amount of memory required. Therefore molecular dynamics methods are not used it has overwhelming theoretical and numerical difficulties for directly solving of the Boltzmann equation. To circumvent the difficulty of a direct solution of the Boltzmann equation, DSMC is alternative technique and proposed by Bird [19]in 1963. DSMC accomplishes this through a Monte Carlo integration of the formula for the bi-molecular collision rate, as well as a Monte Carlo integration of

collision dynamics.

2.1.2 DSMC Method

The DSMC technique consists of tracking molecules through physical space and any resultant molecular or boundary interactions. An important assumption in the DSMC formulation is that the gas is dilute or the mean molecular diameter is much less than the mean molecular spacing of molecules in the gas. This allows the molecule motion to be decoupled from the molecular collisions and as such, they are treated as two distinct computational steps. DSMC uses a much smaller set of representative molecules that can be referred to as simulated molecules. Each simulated molecule may represent millions upon millions of actual molecules. Even so, DSMC simulations can vary in size from tens of thousands of simulated molecules for very rarefied two dimensional problems.

Simulation time is discretized into time steps, during which the movement and collision phases of the methodology take place. In the move phase the molecule positions are updated based on the velocity of each individual molecule and the size of the time step. As the molecules traverse the physical space, individual interactions with any surface geometry or domain boundaries must be handled accordingly. Collisions with surfaces can be treated as being either fully specular, fully diffuse or some combination of the two. Specular collisions involve a simple reversal of the molecule velocity component normal to the incident surface. Diffuse collisions cause a random reorientation of the reflected molecule, where the post collision velocity is related to the temperature of the surface.

In the collision phase of the procedure, molecular interactions are treated probabilistically rather than deterministically. The collision procedure takes place on a cell by cell basis, where collision partners are selected from common groups. The time step, volume of the cell, and the number of molecules resident in the cell will determine the number of candidate collision pairs that will be evaluated. The molecules for each candidate collision pair are then chosen at random from the list of molecules in the cell. The relative velocity of the two molecules from each pair is used, in conjunction with the VHS model of Bird [19]. To determine whether the two molecules will collide. The number of candidate collision pairs and the collision probability are formulated such that the proper collision statistics are generated. Once two molecules are chosen, the collision mechanics may involve a redistribution of energy among the kinetic and internal modes of the participating molecules.

In the strictest sense, the size of the flow field cells should relate to the mean-free-path of the local molecules. This stands to reason, since the cells are used to group molecules into candidate collision pairs. If molecules, which are separated by distances much larger than a mean-free-path, are allowed to collide, this would allow a non-physical transfer of mass,

momentum and energy. Similarly, the time step size for the simulation needs to be limited such that it is on the order of the mean time between collisions for the local molecules. If the time step is too large, the molecules will be able to move too far without the opportunity to participate in a collision. This will again cause a smearing of the properties of the flow, resulting in non-physical results. While each of these restrictions could be relaxed in regions where flow gradients are small, such regions are difficult in practice to determine a priority. Excessive temporal and spatial discretization should also be avoided, as this will degrade the performance of the method. One additional requirement of the methodology is that each cell be populated with some minimum number of molecules typically 10-20, so that the proper collision statistics can be maintained.

Another principal phase in the DSMC method is sampling. Since the simulation is performed at the microscopic level, the microscopic properties need to be evaluated to create the more familiar macroscopic properties, such as density, velocity and temperature. The relations for this conversion may be found in Bird [19]. Since many fewer molecules are being simulated than exist in the real gas, there will be significant statistical noise in an instantaneous sample. Successive sampling is done to increase the sample size and thus reduce the statistical noise. Although the flow is always considered unsteady, two means of performing sampling are used for steady-state and time accurate simulations. For steady-state problems, the sampling method is known as time averaging. This involves periodic sampling of the microscopic flow properties once a pseudo steady-state condition is reached in the simulation. Time accurate problems require an ensemble averaging sampling method. In this case, distinct sampling information is maintained throughout the simulation, and the simulation is repeatedly run in order to build up the sample size. In either case, the statistical scatter will decrease with the square root of the sample size. Sampling is also done for the evaluation of macroscopic surface quantities such as pressure, shear stress and heating. In this case, microscopic quantities are tracked at the molecular level for discrete surface elements. Unlike the flow field sampling, which takes place periodically, the surface sampling is done on an event by event basis. The total change of molecular momentum over a given sampling period provides the local force on that element. The pressure can then be obtained by dividing by the area of the sampling element.

The steps in a DSMC simulations can be summarized as follows. The domain is first initialized as a vacuum or uniform equilibrium flow for simplicity. Second step new particles are introduced to the simulation at the inlet boundary of computational domain. Third step is molecule movement. In this step, molecules change positions according to their velocities. Molecules are reflected when they interact with the wall type boundaries. Reflections are realized according to the model chosen. If molecules leave the flow area from the open boundaries, they are just deleted. Meanwhile new molecules are introduced from the open

boundaries at each time step. The numbers and energies of these new molecules depend on the boundary conditions. The fourth step is molecule indexing. Molecules are indexed based on their cell information. The aim of this step is to determine which cell molecules are positioned in. The molecules in the same cell are called neighboring molecules. The fifth step is molecule collisions. Here, some molecules in the same cell undergo collisions with each other. These molecules exchange momentum and energy. But it is assumed that their positions don't change during collisions. The sixth step is sampling the flow and calculation of macroscopic properties. In this step, macroscopic properties in each cell are calculated using microscopic molecule information. Time averaging and ensemble averaging are used in steady and unsteady flows respectively.The process is repeated, as shown in Fig.2.2.

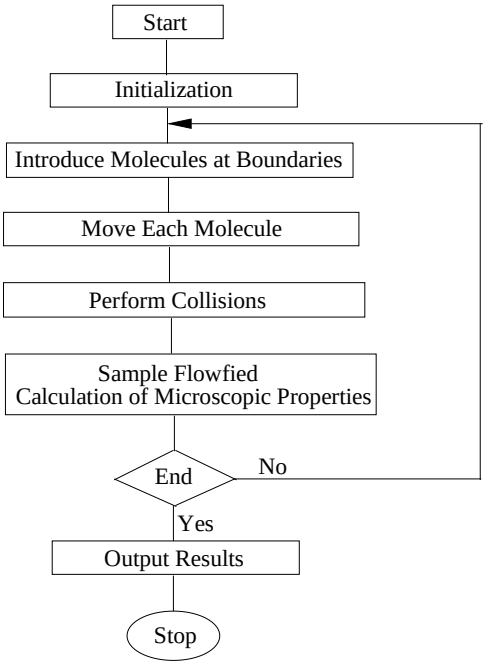

Figure 2.2: Flow chart of DSMC method

2.2 Numerical Method for low density region

Two dimensional unsteady flow over a re-entry vehicle is numerically simulated by solving Boltzmann equation. DS2V software is used to solve the Boltzmann equation developed by Bird based on Direct Simulation Monte Carlo (DSMC) method.

2.2.1 DS2V software

DS2V is a fluid flow solver developed by Bird based on DSMC method for solving 2D planer and asymmetrical flows with high Knudsen number and it is coded in FORTRAN 95. DS2V has inbuilt surface specification windows for geometry drawing. Geometry is drawn by in terms of lines and arcs. Program itself do grid generation and take require number of cells and sampling molecules as per memory set in input parameter windows. Flow domain is drawn as rectangular bounding box by providing max and minimum X and Y coordinate. Input parameter for the flow properties at boundary conditions are set in main stream window in terms of temperature, number density, velocity components and fractions of spices. Program is inbuilt with different gas molecules properties and program setter has to choose particular required gas molecular. DS2V is also employs realistic gas models, gas- surface interactions, gas phase surface reaction and chemical reactions. Geometry and input data can be saved as DS2VD.DAT files. These file can be modified at requirement.

Calculations are done by DS2 code and it can be executable in DS2V program main window or in command prompt terminal.Calculations are done by DS2 code and it can be executable in DS2V program main window or in command prompt terminal. It gives three options to programmer to start calculations: (1) To continue the current run. (2) To adapt cells then continue. (3) To start new run. DS2V is mainly solved problem by unsteady method. After each time step, it writes DS2FF.DAT file. This is further can be used for post processing work.DS2V has interactive flow display panel that can be used for Post processing requirement. Interactive flow display panel can use to check run online by three display panels.first display is used for getting information like simulation time, the maximum and averaged value ofmcs/λ number of simulated molecules, number of collisions and so on.A graphic shows the time history of the number of molecules. Fluctuations are indicative of a stabilization of the run. Second display gives 2D plots of flow parameters such as pressure, Temperature, velocity, density, Mach number and so on. Plots of surface parameters of heat flux, slip velocity, pressure and so on as functions of curvilinear abscissa in third display panel. DS2V allows the user to check the quality of results by means of the display of the maximum and averaged values of the ratio of the mean collision separation (mcs) to the local mean free path (λ). Bird suggests 0.2 as a limit value of mcs/λ for an optimal quality of the run.

DS2V is inbuilt with ideal air and real air. Real gas model is made of five chemical spices: O_2,N_2,O,N,NO in thermo chemical non equilibrium. This real gas model relay on park model. [30]

2.2.2 Park model

The five chemical species ($O_2, N_2, O, N$and NO) react according to 17 forward/reverse chemical reactions by the Park models. For the park model, both the forward (k_f) and the reverse (k_r) rate coefficients are expressed as,

$$k_{f,r} = C_{f,r} T^{n_{f,r}} exp(\frac{-Ea_{f,r}}{KT}) \tag{2.4}$$

where C is the pre-exponential factor in $m^3/molecules/s$, n is the temperature exponent, Ea is the specific activation energy, K is the Boltzmann constant, subscripts f and r stand for forward and reverse reactions. The reactions are reported in Table 2.1 together with the reaction rate coefficients, the ratios of activation energies and the Boltzmann constant. Reactions 1 to 15 are for dissociations/recombinations and 16 to 17 are exchanges reactions.

No	Reactions	C_f	n_f	$Ea_f/k(K)$	C_r	n_r	$Ea_r/k(K)$
1	$O_2 + N \leftrightarrow O + O + N$	5.99×10^{-12}	-1	59500	8.30×10^{-45}	-0.5	0.0
2	$O_2 + NO \leftrightarrow O + O + NO$	5.99×10^{-12}	-1	59500	8.30×10^{-45}	-0.5	0.0
3	$O_2 + N_2 \leftrightarrow O + O + N_2$	1.20×10^{-11}	-1	59500	1.66×10^{-44}	-0.5	0.0
4	$O_2 + O_2 \leftrightarrow O + O + O_2$	5.39×10^{-11}	-1	59500	7.47×10^{-44}	-0.5	0.0
5	$O_2 + O \leftrightarrow O + O + O$	1.55×10^{-10}	-1	59500	2.07×10^{-43}	-0.5	0.0
6	$N_2 + O \leftrightarrow N + N + O$	3.18×10^{-13}	-0.5	113200	3.01×10^{-44}	-0.5	0.0
7	$N_2 + O_2 \leftrightarrow N + N + O_2$	3.18×10^{-13}	-0.5	113200	3.01×10^{-44}	-0.5	0.0
8	$N_2 + NO \leftrightarrow N + N + NO$	3.18×10^{-13}	-0.5	113200	3.01×10^{-44}	-0.5	0.0
9	$N_2 + N_2 \leftrightarrow N + N + N_2$	7.97×10^{-13}	-0.5	113200	7.51×10^{-44}	-0.5	0.0
10	$N_2 + N \leftrightarrow N + N + N$	6.90×10^{-8}	-1.5	113200	6.42×10^{-39}	-1.5	0.0
11	$NO + N_2 \leftrightarrow N + O + N_2$	6.59×10^{-10}	-1.5	45500	2.78×10^{-40}	-1.5	0.0
12	$NO + O_2 \leftrightarrow N + O + O_2$	6.59×10^{-10}	-1.5	75500	2.78×10^{-40}	-1.5	0.0
13	$NO + NO \leftrightarrow N + O + NO$	1.32×10^{-8}	-1.5	75500	5.57×10^{-39}	-1.5	0.0
14	$NO + O \leftrightarrow N + O + O$	1.32×10^{-8}	-1.5	75500	5.57×10^{-39}	-1.5	0.0
15	$NO + N \leftrightarrow N + O + N$	1.32×10^{-8}	-1.5	75500	5.57×10^{-39}	-1.5	0.0
16	$NO + O \leftrightarrow O_2 + N$	5.28×10^{-21}	1.0	19220	1.60×10^{-18}	0.5	3580
17	$N_2 + O \leftrightarrow NO + N$	1.12×10^{-16}	0.0	38400	2.49×10^{-17}	0.0	0.0

Table 2.1: Park kinetic model Reactions

2.3 Numerical formulation in high density Region

2.3.1 Governing equations

The governing equations are derived from conservation laws and the second law of thermodynamics. The conservation equations for turbulent compressible flows are as follows:

Continuity equation:
Conservation of mass states that the total mass of the universe is constant; in other words, mass is neither created nor destroyed but can only be moved from one place to another.

$$\frac{\partial \rho}{\partial t} + \frac{\partial}{\partial x_j}[\rho u_j] = 0, \qquad j = 1, 2, 3 \tag{2.5}$$

Momentum equation:
Conservation of momentum says that momentum changes due to one of three factors - redistribution, conversion of momentum to or from energy, and force. In other words, if momentum increases in one place, either momentum or an equivalent amount of energy must decrease someplace else, or a force must act.

$$\frac{\partial}{\partial t}(\rho u_i) + \frac{\partial}{\partial x_j}[\rho u_i u_j + p\delta_{ij} - \tau_{ji}] = 0, \qquad i, j = 1, 2, 3 \tag{2.6}$$

Energy equation:
Conservation of energy says that energy change is due to one of three factors redistribution, conversion of energy to or from momentum, or conversion to or from some other form of energy, heat, or work. In other words, if energy increases in one place, either energy or an equivalent amount of momentum must decrease someplace else, or heating or work must be done.

$$\frac{\partial}{\partial t}(\rho e_0) + \frac{\partial}{\partial x_j}[\rho u_j e_0 + u_j P + q_j - u_i \tau_{ji}] = 0, \qquad i, j = 1, 2, 3 \tag{2.7}$$

Viscous stress is given by:

$$\tau_{ij} = 2\mu S^*_{ij}, \qquad i, j = 1, 2, 3 \tag{2.8}$$

Where the viscous strain rate is defined by,

$$S^*_{ij} = \frac{1}{2}(\frac{\partial \rho u_i}{\partial x_j} + \frac{\partial u_j}{\partial x_i}) - \frac{1}{3}\frac{\partial u_k}{\partial x_k}\delta_{ij}, \qquad i, j = 1, 2, 3 \tag{2.9}$$

Where $\mu = \mu_l + \mu_t$ is the total viscosity; μ_l, μ_t being the laminar and turbulent viscosity.

Laminar viscosity (μ_l) is calculated from Sutherland's law as,

$$\mu_l = \mu_{ref}(\frac{T}{T_{ref}})^{\frac{3}{2}}\frac{T_{ref}+S}{T+S} \tag{2.10}$$

T_{ref} is a reference temperature.
μ_{ref} is the viscosity at the T_{ref} reference temperature
S is the Sutherlands Coefficient.

Specific as function of temperature for air is given by,
For $200 \leq T < 1000$

$C_p = 1161.482 - 2.368814T + 0.01485511T^2 + -2.034909 \times 10^{-5}T^3 + 9.928569 \times 10^{-8}T^4 - 1.111097 \times 10^{-10}T^5$

$For 1000 \leq T < 3000$

$C_p = -7069.814 + 33.70605T - 0.0581276T^2 + 5.421615 \times 10^{-5}T^3 - 2.936679 \times 10^{-8}T^4 + 9.237533 \times 10^{-12}T^5$

And,

$$\gamma = \frac{C_p}{C_v} \tag{2.11}$$

$$P = \rho RT \tag{2.12}$$

The Spalart-Allmaras turbulent model is a relatively simple one-equation model that solves a modeled transport equation for the kinematic eddy (turbulent) viscosity. This embodies a relatively new class of one-equation models in which it is not necessary to calculate a length scale related to the local shear layer thickness. The Spalart-Allmaras model was designed specifically for aerospace applications involving wall-bounded flows and has been shown to give good results for boundary layers subjected to adverse pressure gradients. It is also gaining popularity in the turbomachinery applications.

The model proposed by Spalart and Allmaras solves a transport equation for a quantity that is a modified form of the turbulent kinematic viscosity.

The transported variable in the Spalart-Allmaras model, $\overline{\nu}$, is identical to the turbulent kinematic viscosity except in the near-wall (viscosity-affected) region. The transport equation for $\overline{\nu}$ is,

$$\frac{\partial}{\partial t}(\rho\overline{\nu}) + \frac{\partial}{\partial x_i}(\rho\overline{\nu}u_i) = G_\nu + \frac{1}{\sigma_{\overline{\nu}}}\left[\frac{\partial}{\partial x_j}\left\{(\mu + \rho\overline{\nu})\frac{\partial\overline{\nu}}{\partial x_j}\right\} + C_{b2}\rho\left(\frac{\partial\overline{\nu}}{\partial x_j}\right)^2\right] - Y_\nu + S_{\overline{\nu}} \quad (2.13)$$

where G_ν is the production of turbulent viscosity and Y_ν is the destruction of turbulent viscosity that occurs in the near-wall region due to wall blocking and viscous damping. $\sigma_{\overline{\nu}}$ and C_{b2} are the constants and ν is the molecular kinematic viscosity. $S_{\overline{\nu}}$ is a user-defined source term. Note that since the turbulence kinetic energy k is not calculated in the Spalart-Allmaras model, while the last term in Equation is ignored when estimating the Reynolds stresses.

The turbulent viscosity μ_t is computed from,

$$\mu_t = \rho\overline{\nu}f_{\nu 1} \quad (2.14)$$

where the viscous damping function $f_{\nu 1}$ is given by,

$$f_{\nu 1} = \frac{\chi^3}{\chi^3 + C_{\nu 1}^3} \quad (2.15)$$

and

$$\chi = \frac{\overline{\nu}}{\nu} \quad (2.16)$$

The destruction term is modeled as,

$$Y_\nu = C_{w1}\rho f_w\left(\frac{\overline{\nu}}{d}\right)^2 \quad (2.17)$$

where

$$f_w = g\left[\frac{1 + C_{w3}^6}{g^6 + C_{w3}^6}\right]^{\frac{1}{6}} \quad (2.18)$$

$$g = r + C_{w2}(r^6 - r) \quad (2.19)$$

$$r = \frac{\overline{\nu}}{\overline{S}k^2d^2} \quad (2.20)$$

$$\overline{S} = S + \frac{\overline{\nu}}{k^2d^2}F_{\nu 2} \quad (2.21)$$

$$f_{\nu 2} = 1 - \frac{\chi}{1 + \chi f_{\nu 1}} \quad (2.22)$$

C_{b1} and k are constants ,d is the distance from the wall,and S is a scalar measure of the deformation tensor as proposed by Spalart and Allmaras. S is based on the magnitude of

the vorticity,

$$S = \sqrt{2\Omega_{ij}\Omega_{ij}} \tag{2.23}$$

whereΩ_{ij} is the mean rate-of-rotation tensor and is defined by

$$\Omega_{ij} = \frac{1}{2}\left(\frac{\partial u_i}{\partial x_j} - \frac{\partial u_j}{\partial x_i}\right) \tag{2.24}$$

Corresponding constants are given by,

$$C_{b1} = 0.1355$$
$$C_{b2} = 0.622$$
$$\sigma_{\overline{\nu}} = \frac{2}{3}$$
$$C_{\nu 1} = 7.1$$
$$C_{w1} = \frac{C_{b1}}{k^2} + \frac{(1+C_{b2})}{\sigma_{\overline{\nu}}}$$
$$C_{w2} = 0.3$$
$$C_{w2} = 2.0$$
$$k = 0.4187$$

2.4 Numerical method for high density region

Two dimensional unsteady compressible turbulent flow equations are solved using commercial CFD software FLUENT. Spalart-Allmaras turbulent model used for modeling turbulence. Air is considered as an ideal gas with variable properties. Sutherland's law is used to calculate the viscosity and piece wise polynomial is used to calculate temperature dependent specific heat. The boundary conditions at the inflow are specified as pressure far field for setting free stream operating conditions and the flow variables at the outflow are extra polated from the interior as by setting the boundary as pressure outlet. No-slip boundary conditions are imposed at the solid walls for velocity field. Constant wall temperature boundary condition is used to obtain heat flux on the surface of wall. A fine grid is done near to the wall of the re-entry vehicle in order to capture the Shock.

2.4.1 Pre-processing

Pre-processing is divided into two stages Geometry and Meshing. It is carried out using ANSYS ICEM CFD 13.0. Geometries details of the Orion CEV vehicle are given in Fig.1.4 are used to model geometry. To study the flow field analysis over the re-entry vehicle, rectangular box is drawn. At geometry drawing, meshing operation is performed by using ANSYS ICEM CFD 13.0.A blocking strategy used to split geometry in to several blocks. O grid tool is used to make structured grid around the re-entry vehicle body. More denser

grid around the re-entry vehicle body compare to away part from body to capture the strip variation in properties.

Chapter 3

Results for Low density region

3.1 Validation

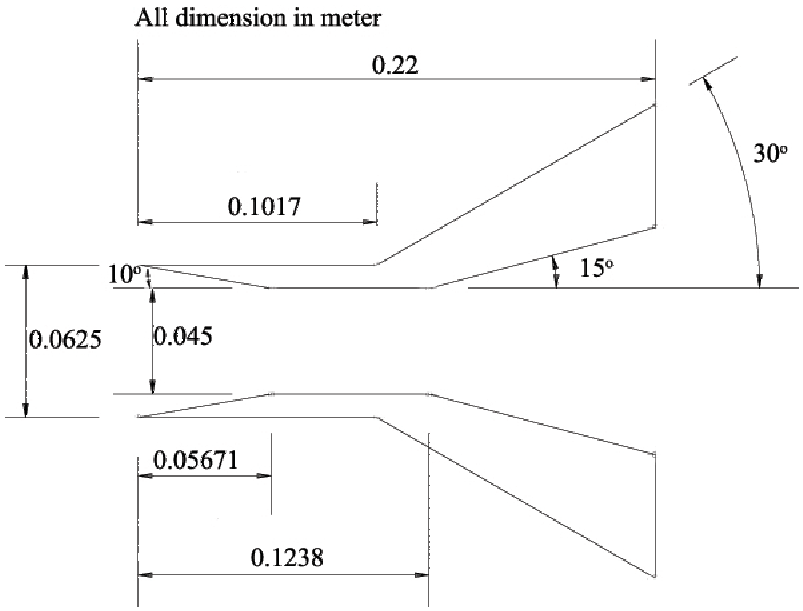

Figure 3.1: Schematic diagram of hollow cylinder flare

In order to tune the DSMC method described in chapter 2 for prediction of hypersonic flow over Orion CEV vehicle in very low density rarefied regime, a classical experimental test case dealing with shock-wave/boundary layer interaction, namely the hollow cylinder flare, has been performed. Fig.3.1 is showing the schematic diagram of the hollow cylinder flare. The hollow cylinder flare is characterized by a sharp leading edge with a bevel angle of 15^o. The compression flare is inclined by 30^o. with respect to the cylinder and is followed by a hollow cylindrical section. The model total length is 0.22 m and the reference length L is same 0.1 m.

The experimental was carried out on hollow cylinder flare in Large Energy National Shock (LENS) tunnel at CALSPAN Buffalo Research Center (CUBARC) by Ambrosio [31]. RUN 11 experimental is choosen for the validation study and simulated in DS2V software. Perfect Nitrogen gas is taken as flow fluid. Free stream conditions are taken: velocity U_∞=2609 m/s, Temperature T_∞ =128.9 K, Number Density$n_\infty = 1.090 \times 10^{22}$, density ρ_∞=$5.07 \times 10^{-4} Kg/m^3$, Mach number $M_\infty = 11.1$ pressure P_∞=19.405 Pa. No slip conditions are given on walls of the hollow cylinder flare and kept at constant wall temperature $T_w = 297.2K$.

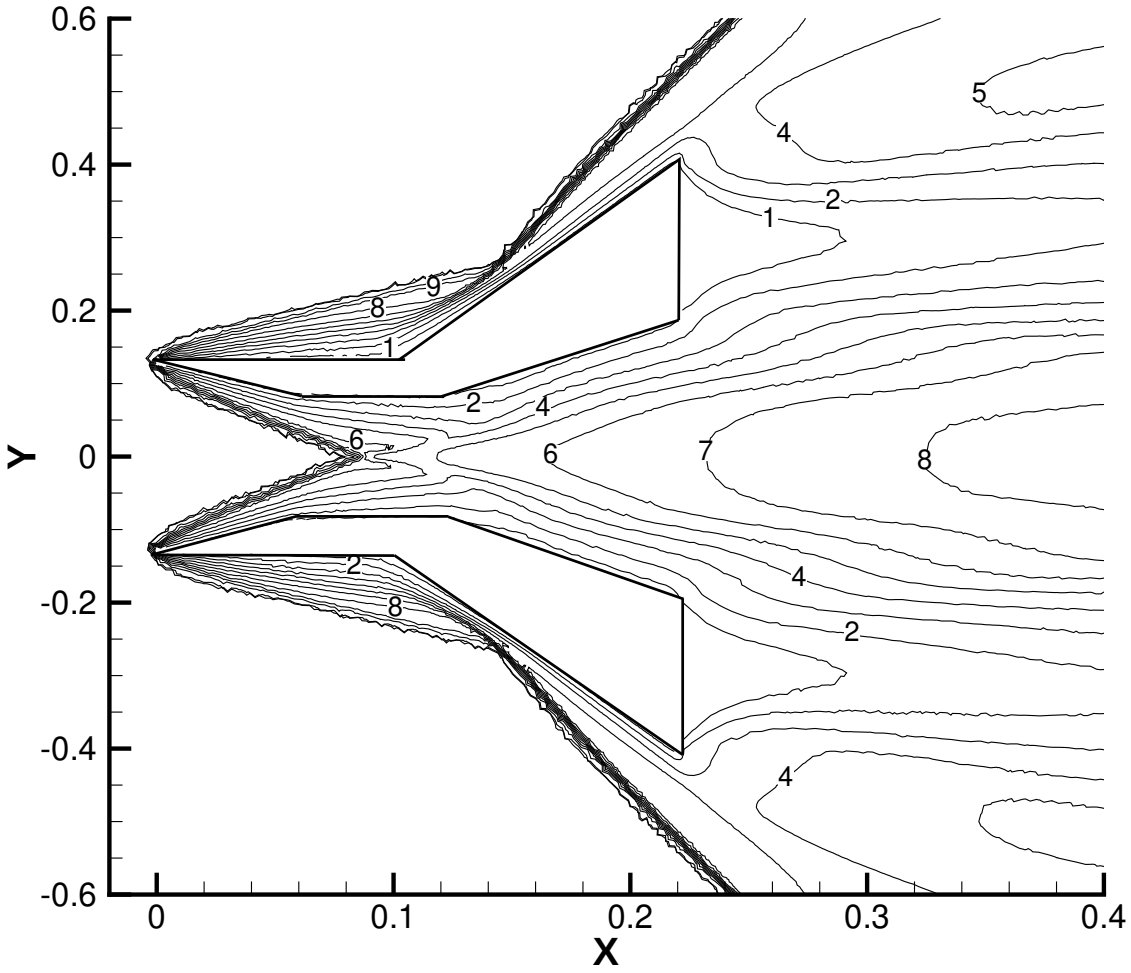

Figure 3.2: Mach number contours

Mach contours over on hollow cylinder flare are obtained with the above operating con-

ditions and shown in Fig.3.2. From Fig.3.2, one can notice that weak shock at the leading edge and strong shock at the hinge of flare. The leading edge shock and flare shock merging at a particular point and forms a reflected shock along the flare. Present numerical methods are captured the experimental observations such as interactions between shock waves and boundary layers and also the interflow characteristics through hollow cylinder flare. Due to increase in area expansions is happen in inner hollow portion and Mach number is also increase.

Fig.3.3(a & b) give quantitative comparison between present results and experimental results. The wall pressure and heat flux distribution along the outer wall surface of the hollow cylinder flare is represented in dimensionless form as pressure coefficient (C_p) and Stanton number (S_t) are defined as

$$C_p = \frac{P - P_\infty}{0.5\rho_\infty {U_\infty}^2} \tag{3.1}$$

$$S_t = \frac{q}{0.5\rho_\infty {U_\infty}^3} \tag{3.2}$$

From Fig.3.3(a), one can notice that initial decrease of pressure coefficient due to the strong viscous interaction and increase of pressure coefficient due to the flare deflection angle which creates the strong flare shock. The leading edge shock and flare shock merges at a particular point which indicates the maximum pressure coefficient. Pressure coefficientC_p becomes maximum around X=0.14 due to this merging of weak shock and strong shock. The downstream of reflected shock creates an expansion wave due to increase in area, hence the pressure coefficient decreases along the flare wall after merging of shock waves.

From Fig.3.3(b), the Stanton number initially decreases due to viscous boundary layer and then increases due to flare shock. The maximum heat flux is observed on the flare due to merging of leading edge shock and flare shock. Form Fig.3.3, the present results showed an excellent agreement with the experimental results of Ambrosio [31].

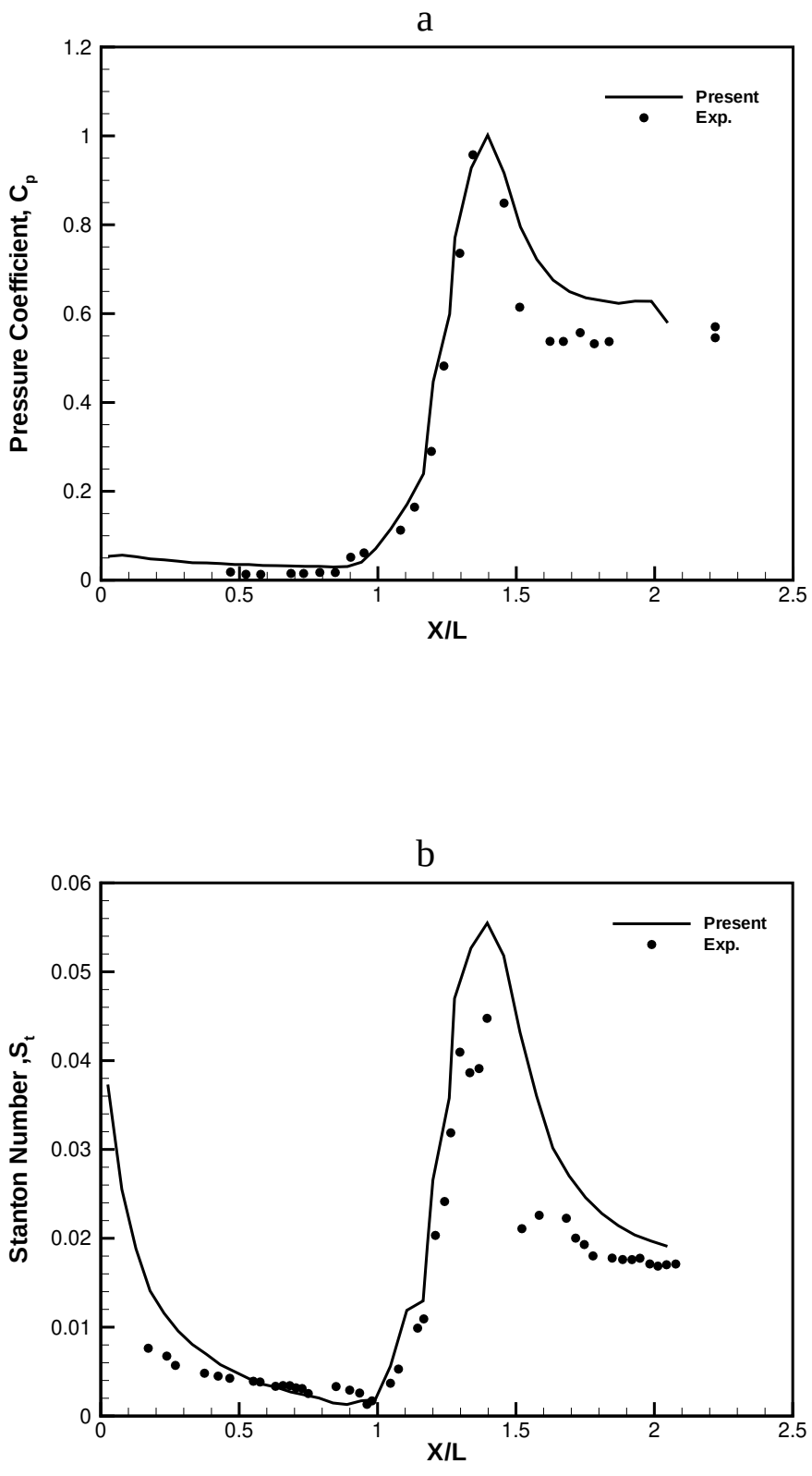

Figure 3.3: Comparison of pressure coefficient and Stanton number with experimental results

3.2 Numerical simulation results and discussion in low density region

Study of flow over a re-entry vehicle involves the complex flow phenomena of hypersonic flow. Now days, CFD is a powerful tool for analyzing the complex flow phenomena of hypersonic flows. Flow analysis of NASAs future space vehicle Orion CEV is done at high altitude in rarefied regime using DS2V software. Unsteady two dimensional axisymmetric Boltzmann equations with radial factor is solved by DSMC method. Simulations are done between 90 km to 125 km with in step of 5 km and corresponding free stream flow properties of air at particular altitude are taken as per US standard atmosphere 1976 data [32] and shown in Table 3.1. Isotherm boundary condition are taken for Wall of the Orion Re-entry vehicle and kept at particular temperature, also no slip boundary are imposed to wall. Temperature of wall are choosen such way that vehicle body maintains at this temperature at particular altitude during the re-entry of the vehicle. wall temperature taken for the particular altitude is shown in Table 3.2. Sufficient large domain over entry vehicle body taken in order to analysis flow over the body.

Air is modeled as ideal(perfect) gas and real gas. Ideal air is assumed to made of nitrogen and oxygen with mass fraction of 0.79 and 0.21 respectively. Oxygen and Nitrogen dissociation start at high temperature. During the re-entry of Orion vehicle very high temperature generated around the re-entry vehicle body. Flow is in non equilibrium and chemically reacting during at these high temperature. In order to take the effect of this chemical reactions like dissociation,recombination and non equilibrium air is modeled as real air. It is assumed that real air is made of five spices named O_2, N_2, O, N and NO. Fractions of the each spices are shown in Table 3.1. 17 forward and backward chemical kinematics reactions are taken in order to modeling of dissociation and recombination modeling based on park model as explained in chapter 2.

Flow field characteristics and peak heat flux for different altitudes in the rarefied regime are reported here. The effects of nose radius and free stream velocity are also reported here.

H(km)	T(K)	P(Pa)	$\rho(K_g/m^3)$	n$(1/m^3)$	X_{N_2}	X_{O_2}	X_O	X_{A_r}	X_{H_e}
90	186.870	0.1836	3.24×10^{-6}	7.1160×10^{19}	0.7795	0.2078	0.0034	0.0092	0.0000
95	188.420	0.0760	1.39×10^{-6}	2.9200×10^{19}	0.7766	0.1996	0.0149	0.0080	0.0000
100	195.080	0.0320	5.60×10^{-7}	1.1890×10^{19}	0.7749	0.1810	0.0362	0.0080	0.0000
105	208.840	0.01456	2.33×10^{-7}	5.0210×10^{18}	0.7733	0.1523	0.0673	0.0066	0.0000
110	240.000	0.0071	9.71×10^{-8}	2.1440×10^{18}	0.7654	0.1223	0.10744	0.0049	0.0000
115	300.000	0.0040	4.26×10^{-8}	9.6810×10^{17}	0.7493	0.0996	0.1475	0.0035	0.0000
120	360.00	0.0025	2.22×10^{-8}	5.1070×10^{17}	0.7296	0.0861	0.1816	0.0027	0.0001
125	417.230	0.0017	1.29×10^{-8}	3.013×10^{17}	0.7086	0.0775	0.2116	0.0022	0.0001

Table 3.1: Properties of air from US Standard Atmosphere 1976

H(km)	M_a at 7.5 Km/s	M_a at 11.0 Km/s	T_w
90	27.37	40.16	1065
95	27.26	39.99	950
100	26.79	39.29	800
105	25.89	37.97	760
110	24.15	35.422	700
115	21.60	31.68	620
120	19.72	28.92	550
125	18.32	26.86	490

Table 3.2: Mach number and wall temperature at different altitude

3.2.1 Ideal and real gas effect

To know the flow characteristics and peak heat flux of Orion CEV re-entry vehicle, results are obtained for different altitudes varies from 90-125 km from earth atmosphere at free stream velocity 7.5 km/s . Air is modeled as ideal gas as well as real gas. The flow characteristics of pressure, temperature and Mach number contours are obtained at steady state conditions.

Temperature contours over an Orion CEV are shown in Fig.3.4. for ideal gas and real gas at an altitude of 100 km. From Fig.3.4 one can say that computed temperature higher for ideal gas case compared to real gas model. It is observed that maximum temperature zone is formed away from the re-entry vehicle nose radius for both ideal and real gas model. It is happened due to the blunt shape of the Orion CEV Re-entry vehicle. Due to blunt shape of the vehicle , air cannot get out of the way quickly enough and acts as an air cushion to push the shock wave and heated shock layer forward(away from the vehicle). Since most of the hot gases are no longer in direct contact with the vehicle, the heat energy would stay in shocked gas. Maximum Temperature is raised up to around 27000 K for ideal gas and 17100 K for real gas model. Maximum temperature zone thickness is higher for ideal gas model compare to real gas model due to no dissociation and recombination effect are taken

in to account in ideal gas model. Temperature decrease at the corners of re-entry vehicle due to expansion fan. In the downstream part also temperature is lower for real gas model compare to ideal gas model.

Mach number contours for free stream velocity 7.5 km/s at altitude 100 km over Orion CEV vehicle are plotted at steady state condition for both ideal and real gas are shown in Fig.3.6. From contour prominent feature like bow shock ahead of nose radius is observed. Flow expansion occurs at the corners of Orion CEV re-entry vehicle is visible from the Mach number plot for both ideal and real gas. Flow near the body is in subsonic condition. At corners for same place in flow domain Mach number value higher for real gas model compare to ideal gas due to low temperature in real gas model. However, it is noticed that subsonic zone in down part of flow domain is lower for ideal gas compare to real gas. Mach number contours start compression over re-entry as the altitude decrease and density increase and graph of same are not reported due to repetitions of same graph.

Pressure contour for both ideal and real gas are shown in Fig.3.5 at 100 km altitude at free stream velocity 7.5 km/s. Both models are capturing the bow shock. Maximum generated pressure is same for both model and its value is 30 Pa which is 937.5 times the free stream velocity. The strength of bow shock and distance of the shock from the vehicle is less for real gas case compared to ideal gas.

Surface heat flux distribution along the nose radius from the nose center is shown in Fig.3.7 at an altitude of 100 km for free stream velocity 7.5 km/s. From Fig.3.7, heat flux reaches a maximum in the stagnation region which is at the nose center and then decreases slowly along the nose. Surface heat flux is higher for ideal gas than real gas model. Peak heat flux predicated by ideal gas model is around 61000 W/m^2 and that for the real gas model is nearly 45000 W/m^2.

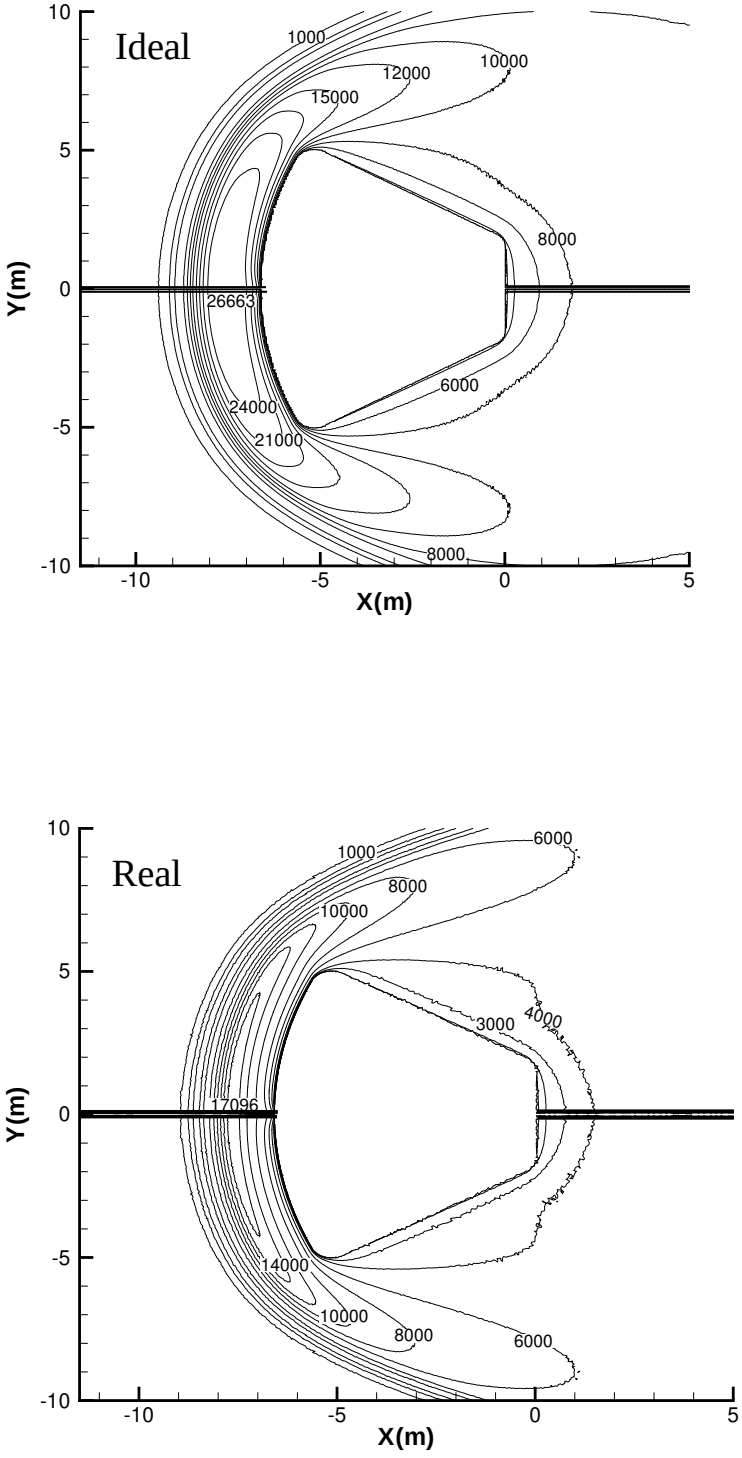

Figure 3.4: Temperature contours at an altitude of 100 km for free stream velocity of 7.5 km/s: (a) ideal gas and (b) real gas.

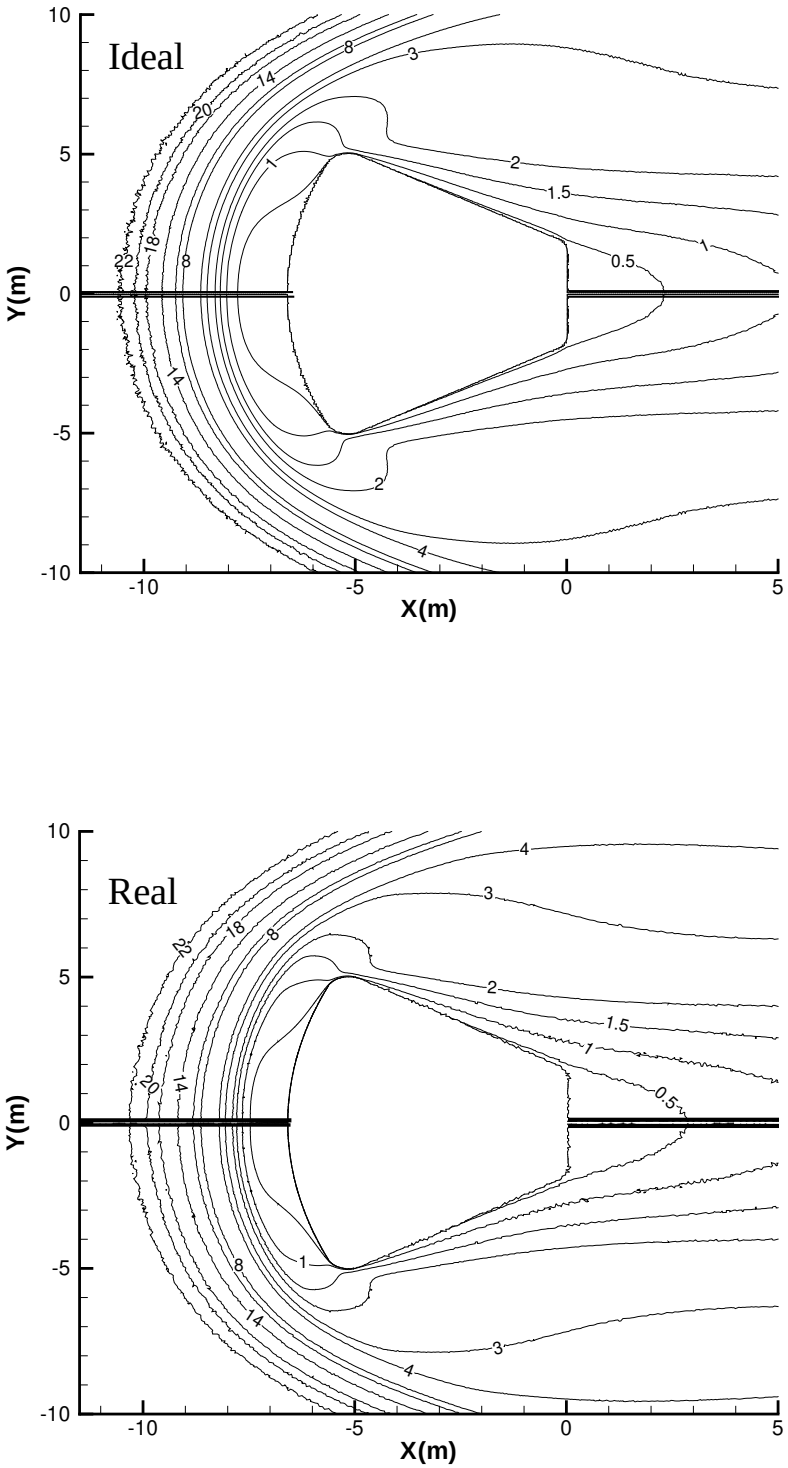

Figure 3.5: Mach number contours at an altitude of 100 km for free stream velocity of 7.5 km/s: (a) ideal gas and (b) real gas.

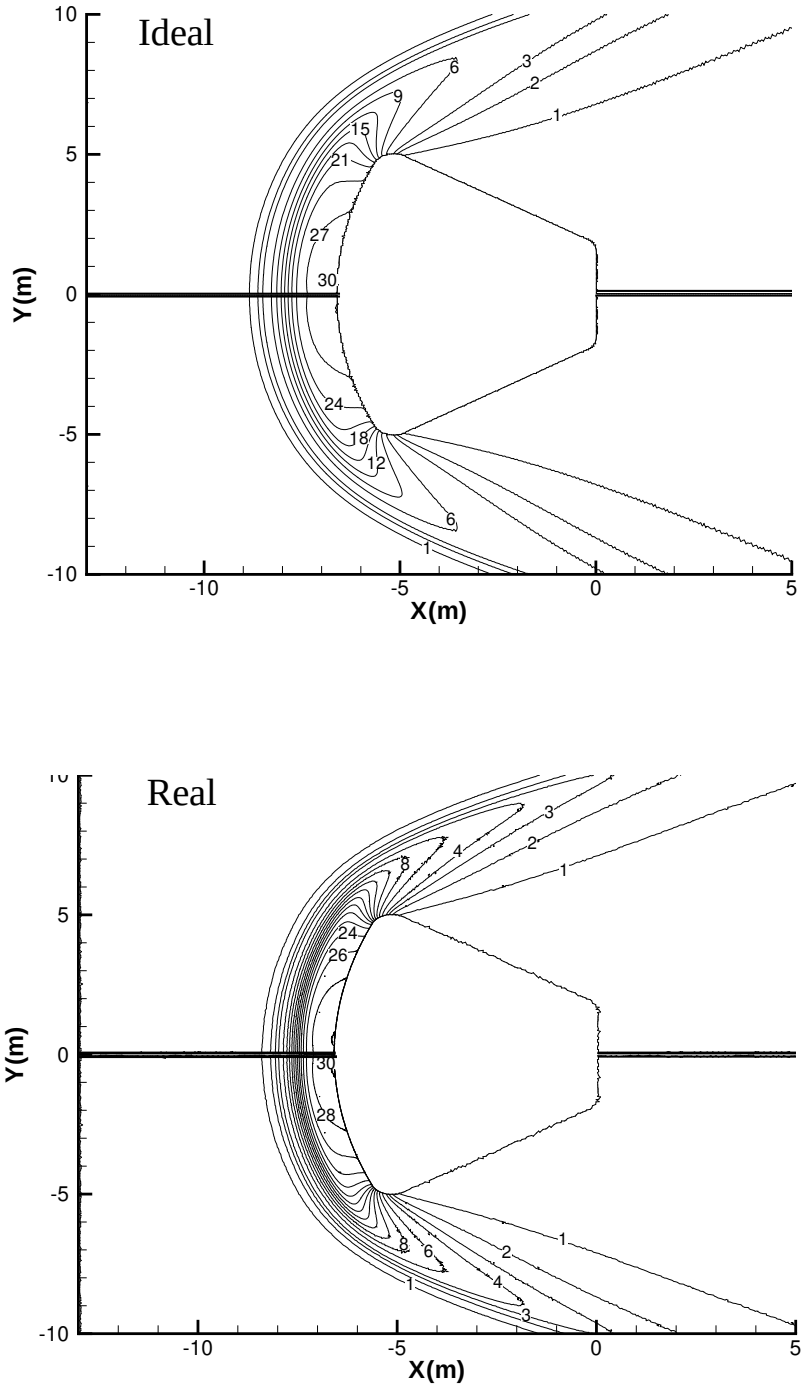

Figure 3.6: Pressure contours at an altitude of 100 km for free stream velocity of 7.5 km/s: (a) ideal gas and (b) real gas.

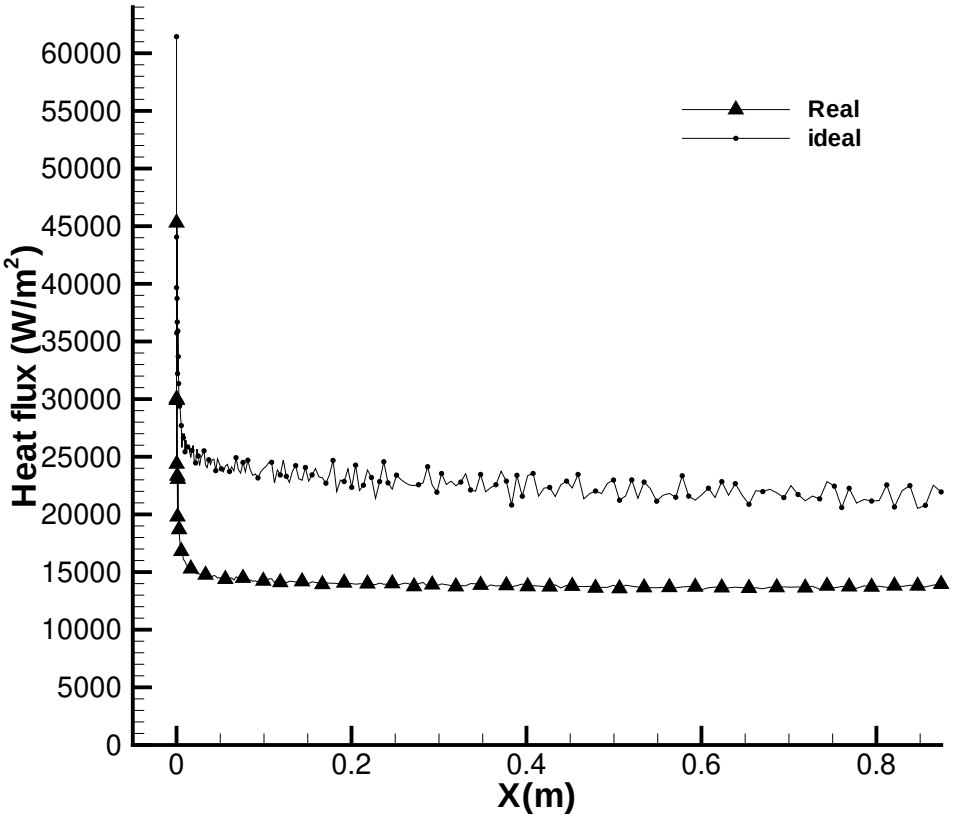

Figure 3.7: Surface heat flux distribution along the nose at an altitude of 100 km for free stream velocity of 7.5 km/s.

3.2.2 Effect of Altitude

Simulations at different altitude with free stream conditions as shown in Table 3.1 and wall temperature as shown in Table 3.2 are done with free stream velocity 7.5 km/s. Peak surface heat flux variation with different altitude is shown in Fig.3.8 for ideal gas and real gas. From Fig.3.8, one can notice that peak surface heat flux increases with decrease in altitude due to increase in density of air. Due to increase in density more friction happen at wall of re-entry and more heat flux generates. The surface heat flux is 33.67 % higher in ideal gas model compared to real gas model approach at an altitude of 100 km. Difference in heat predication by ideal gas and real gas model approaches increase as altitude decrease.

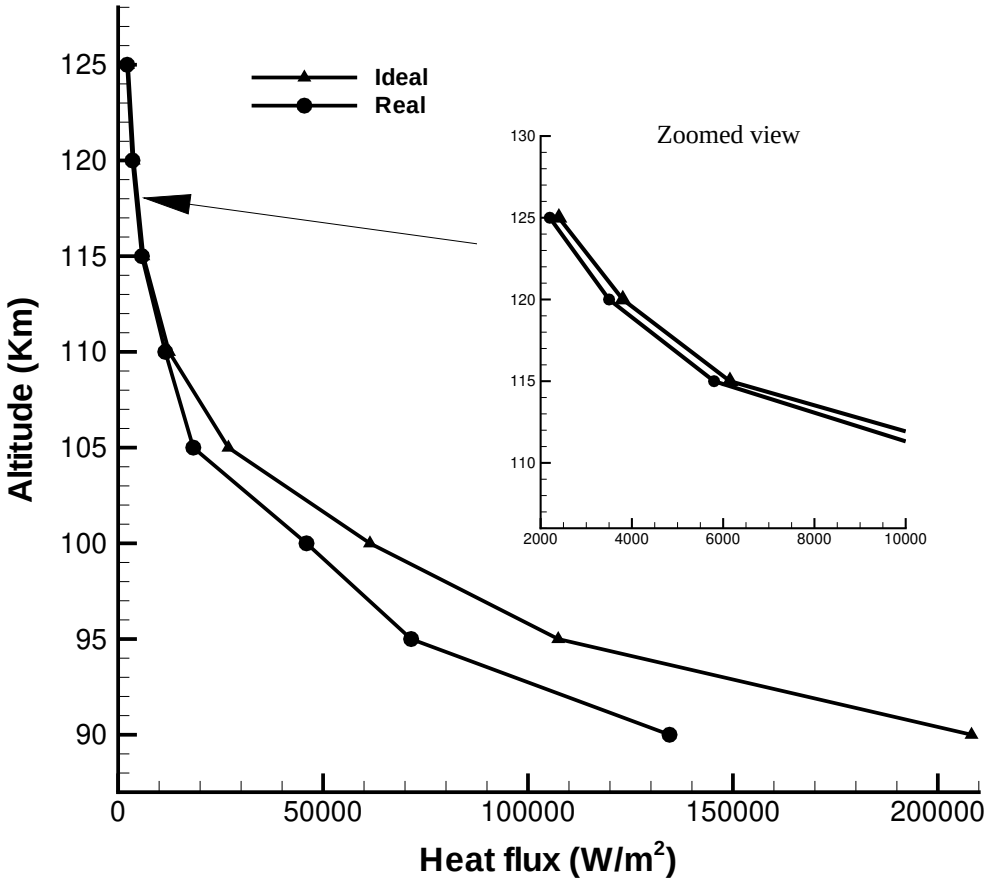

Figure 3.8: Peak heat flux variation with different altitudes at free stream velocity 7.5 Km/s

3.2.3 Effect of free stream Velocity

The design criterion of Orion CEV vehicle re-entry at very high speeds around 11 km/s is given in [12]. To study the effect of free stream velocity, simulations are done at free stream velocity 11 km/s corresponding to free stream properties of air at altitude 100 Km, 110 Km and 120 km. Comparison of flow field characteristic at high free stream velocity 11 km/s is compare with 7.5 km/s at altitude 100 km. Free stream Mach number correspond to 11 Km/s speed is 39.3 and that is for 7.5 km/s is 26.7 for altitude 100 km. Simulations are done for real gas model based on park. Mach contours for high free stream velocity 11 km/s are shown in Fig.3.9. Bow shocks are nicely captured and increase of Mach number occurs at corners due to expansion fan.

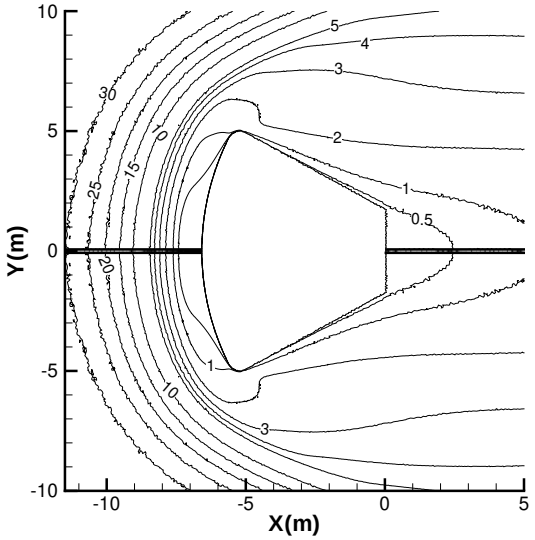

Figure 3.9: Mach number contours at an altitude of 100 km for free stream velocity of 11 km/s.

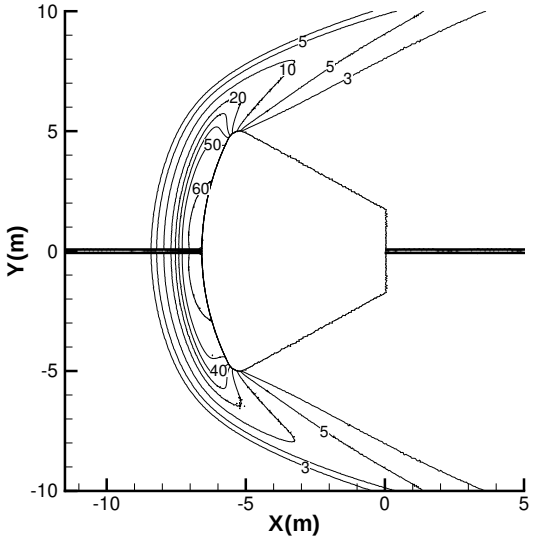

Figure 3.10: Pressure contours at an altitude of 100 km for free stream velocity of 11 km/s.

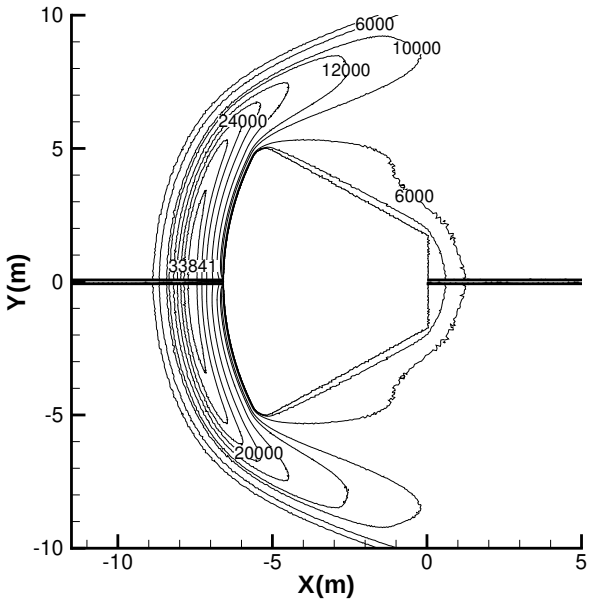

Figure 3.11: Temperature contours at an altitude of 100 km for free stream velocity of 11 km/s.

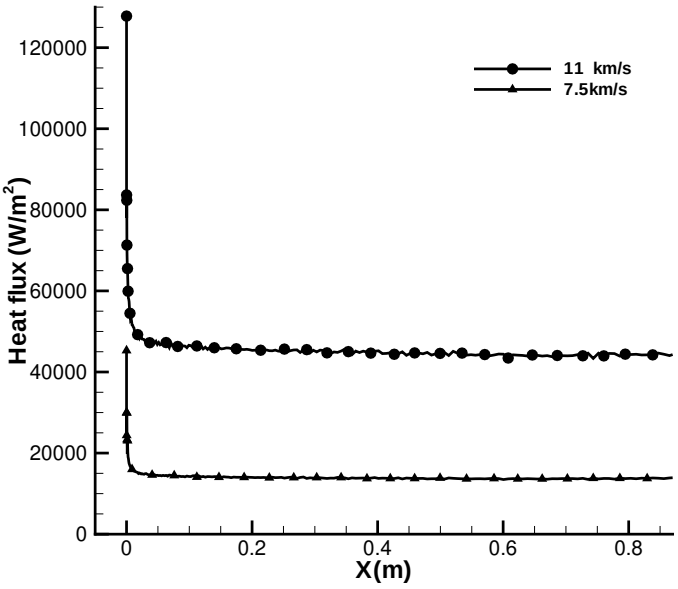

Figure 3.12: Surface heat flux distribution along the nose for different free stream velocity.

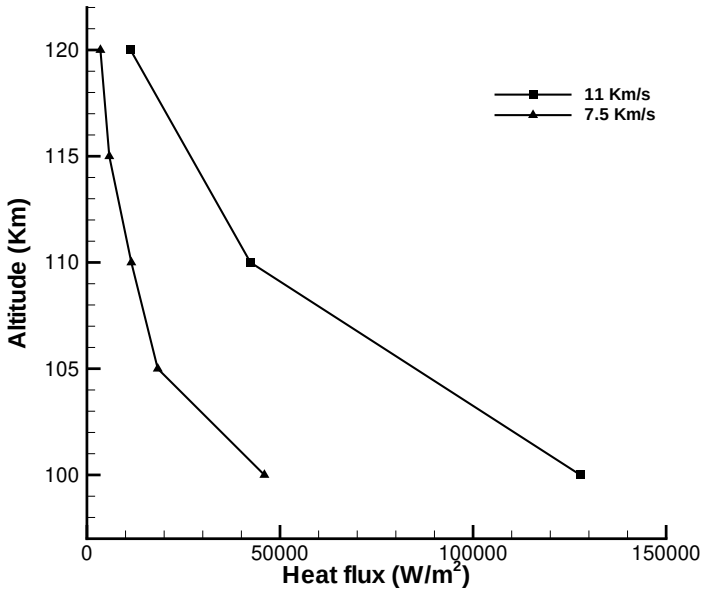

Figure 3.13: Peak heat flux variation with different altitudes.

Pressure contours and temperature contours are shown in Figs.3.10 and 3.11 at altitude of 100 km for real gas model. From Figs.3.10 and 3.11, the pressure and temperature values drastically increase with an increase in free stream velocity from 7.5 km/s to 11 km/s due to increase in strength of bow shock in front of vehicle. Maximum pressure increase from 30 Pa to 60 Pa for increase in velocity 7.5 km/s to 11 km/s. Similarly temperature also becomes nearly double by increasing from 17100 K to 33800 K. It is concluded that shock strength becomes almost double by increasing velocity from 7.5 km/s to 11 km/s.

Predicated heat flux distribution on the surface along nose radius is plotted from center of nose at free stream velocity 11 km/s and compared with 7.5 km/s corresponding to 100 km altitude is shown in Fig.3.12. Surface heat flux increases with an increase in free stream velocity from 7.5 km/s to 11 km/s which shows that aerodynamic heating of the vehicle increases with increase in free stream velocity. Peak surface heat flux variation with different altitude is shown in Fig. 3.13 for different free stream velocities. From Fig.3.13, one can notice that peak surface heat flux increases with decrease in altitude for different free stream velocities.

3.2.4 Effect of nose radius

Aerodynamic heating of blunt shaped re-entry vehicle depends on the curvature of nose. Heat flux generation at nose center stagnation point is directly inversely proportion to

square root of nose radius [27]. In order to study the effect of nose radius increased by 5 cm and 10 cm from current nose radius 12 m of Orion CEV re-entry vehicle as shown in Fig.1.4. Radius is taken up to nose angle 23.04 and from there fillet radius of 0.1 m given at corners and all other geometric remain same.

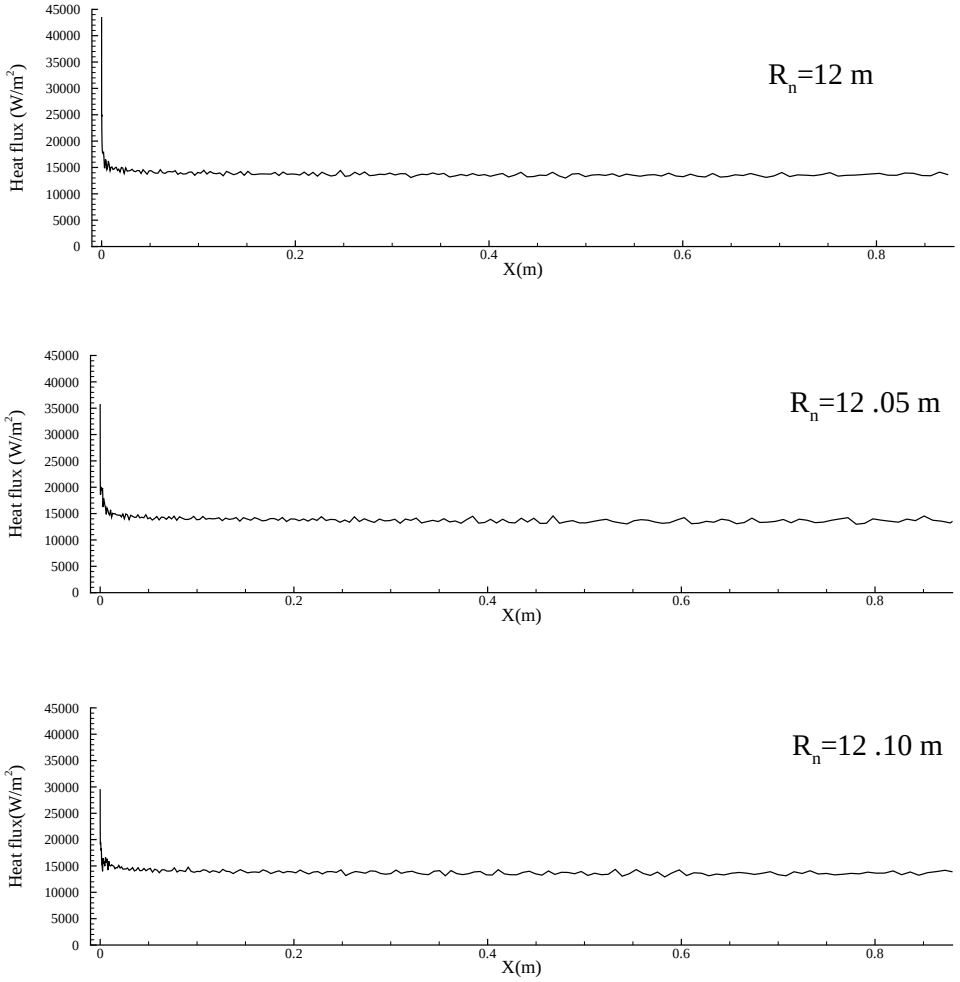

Figure 3.14: Surface Heat flux distribution for different nose radiuses.

The surface heat flux distribution along the nose radius from the nose center is shown in Fig. 3.14 for different nose radiuses at free stream velocity of 7.5 km/s with real gas model at altitude 100 km. Peak heat at nose center decreases with increase in nose radius. It is reported that maximum heat flux at nose center is decreased by 17.83 % for R_n=12.05 m and 32.09 % for R_n=12.10 m when compare to original nose radius R_n=12 m. The surface heat flux is slightly oscillating from the nose center for different nose radiuses and almost same.

Chapter 4

Results in High density region

4.1 Grid independency test

To check that there is no effect of grid sizes on the numerical solution results, Grid independency test is performed. Three different mesh sizes have been simulated corresponding to operating condition of RUN 3073 experiment test. Operating conditions for RUN 3073 are shown in Table 4.2. Meshes are generated with three different grid sizes of coarse mesh 276924 cells, medium mesh 355818 cells and fine mesh 423514 cells. The pressure distribution on the nose radius of re-entry vehicle is normalized with free stream pressure and plotted in Fig.4.1. It is clear that normalized pressure obtained by three different mesh sizes overlapping each other. Quantitative comparison of two different parameter maximum temperature and maximum pressure in bow shock region at three different grid sizes is shown in Table 4.1. It can be seen that solution is grid independent and there is very less variation in the performance parameters for coarse, medium and fine mesh sizes. Hence, medium mesh is chosen for all the simulations reported henceforth.

Grid	Maximum temperature (K)	Maximum pressure (Pa)
Coarse	942.41	973466.6
medium	942.29	973923.7
Fine	942.26	974149.5

Table 4.1: Comparison of different parameters at various grid levels

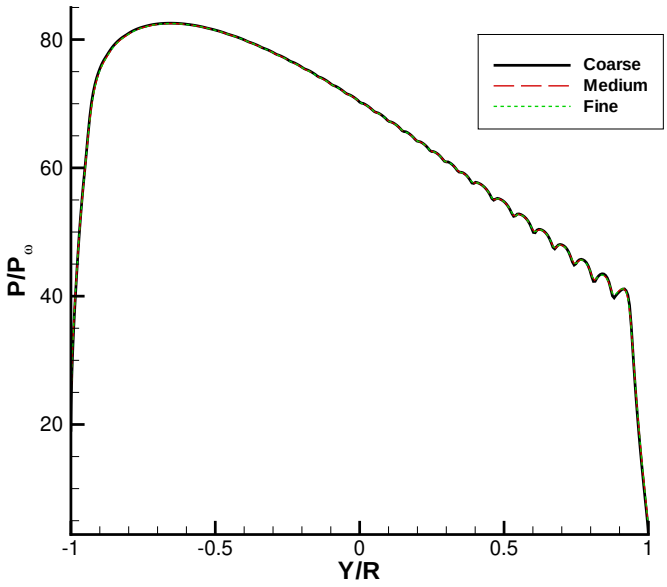

Figure 4.1: Normalized pressure distribution along the nose radius with different grids

4.2 validation

Study of external flow over a re-entry vehicle involves the aerodynamics, thermodynamics analysis. Computational fluid dynamics (CFD) being one of the most powerful tools for understanding various flow phenomena and helps in analyzing the flow field physics and helps in designing and analysis of the re-entry vehicle guiding control and thermal protection System (TPC). The accuracy of present numerical methods is confirmed by validating current numerical methods with the experimental work of Hollis and Bergar et al. [23]. Experimental work on 0.035 scale model of Orion CEV vehicle was done at Arnold Engineering Development Center (AEDC) hypersonic wind tunnel No.9 for Mach 8 and Mach 10. From their experimental work two test case are selected for comparison of present numerical method in high density region. Cases selected are named as RUN 3073 and RUN 3076 with perfect nitrogen as fluid flow. Operating condition of these cases are given in Table 4.2. They measured thermal hating of forebody of Orion vehicle as $S_t \times (Re_\infty)^{1/2}$, and it is defines as,

$$S_t \times (Re_\infty)^{1/2} = \frac{q}{\rho_\infty U_\infty (H_0 - H_w)} \left(\frac{\rho_\infty U_\infty D}{\mu_\infty} \right)^{1/2} \tag{4.1}$$

where,

$$(H_0 - H_w) = \left(C_p T_\infty + U_\infty^2\right) - C_p T_w \tag{4.2}$$

Run	Run 3073	Run 3076
$\alpha(deg.)$	28	28
M_∞	7.96	7.80
P_∞ (Pa)	11800	8400
T_∞ (K)	70.6	75.5
ρ_∞ (Kg/m^3)	0.566	0.376
U_∞ (m/s)	1360	1380
Re_∞	1.57×10^8	9.90×10^7
T_w (K)	330	394

Table 4.2: CEV test conditions for AEDC Tunnel

Numerical simulations are performed with same operating conditions on 0.04 scaled model of Orion CEV re-entry vehicle. Two dimensional unsteady compressible equation with Spalart-Allmaras turbulent modeling are solved. Results of present simulations are presented in terms of Stanton number variation on the fore body (nose radius) of Orion CEV at steady state and also compared with experimental result as shown in Figs. 4.2 and 4.4. The angle of attack is considered in the wind side. From Fig.4.2 , one can notice that minimum value of $S_t \times (Re_\infty)^{1/2}$ is near to the flow incident point due to stagnation condition which corresponds maximum temperature of fluid and minimum heat transfer rate. From incident zone, heat transfer increase and become peak at corner followed by a sharp decrease as the gas temperature drops due to flow expansion. Drop in temperature at corner clearly shown in Fig.4.3. From Figs.4.3 and 4.4, present results showing similar trend and are in good agreement with the experimental results and slight deviations are due to three dimensional effects which are not considered here.

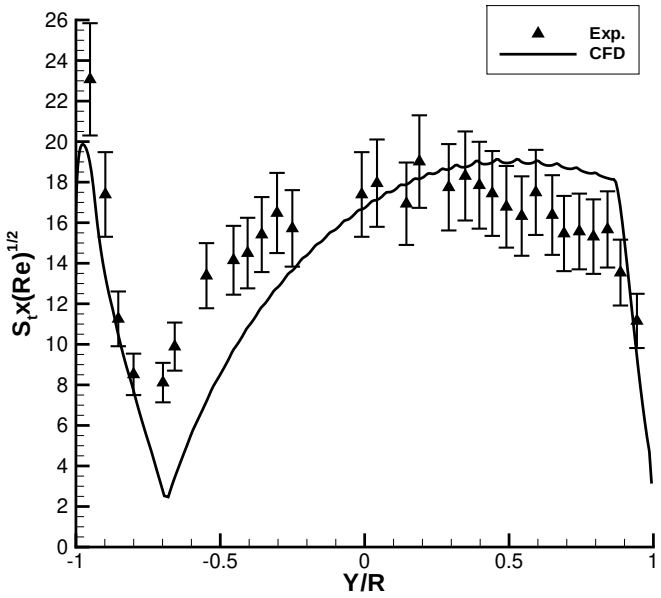

Figure 4.2: Comparison of results for run 3073

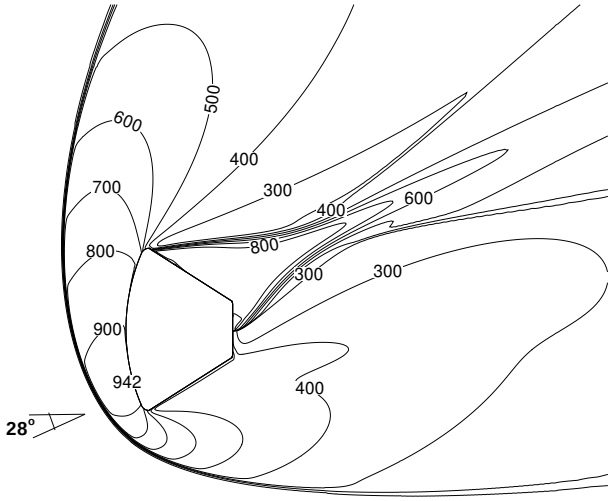

Figure 4.3: Temperature contours for run 3073

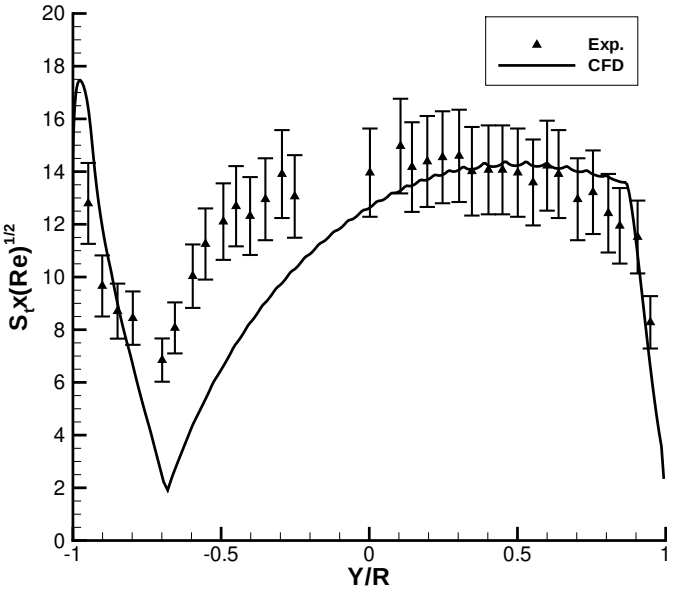

Figure 4.4: Comparison of results for run 3076

4.3 Results in high density region

Analysis of flow behavior over Orion CEV re-entry vehicle in high density region at low altitude 15 km and 20 km is performed for different free stream velocity. Free stream conditions of air at this altitude taken as per US Standard atmosphere 1976 [32] as shown in Table 4.3. 0.04 scaled model of Orion CEV is taken for present study. The no-slip boundary condition at the walls for velocity and constant wall temperature of 1000 K for all cases. Two dimensional unsteady compressible equation with Spalart-Allmaras turbulent modeling are solved using Fluent software. Results are presented at steady state condition.

H(km)	T(K)	P(Pa)	$\rho(Kg/m^3)$
15	216.65	18823	0.30267
20	216.65	5476.5	0.088035

Table 4.3: Properties of air from US Standard atmosphere 1976 in high density region

4.3.1 Effect of Mach number

To know the effect of free stream velocity, results are obtained at an altitude of 15 km with zero angle of attack for different Mach numbers of 8 and 10. Free stream velocity corresponding to Mach 8 conditions is 2400.81 m/s and at Mach 10 conditions is 2996.33

m/s. Mach number distributions over the re-entry vehicle at Mach 8 are shown in Fig.4.5. The main flow features include the bow shock in front of the vehicle, which is symmetric about the body. The shock flow on the body is subsonic with Mach number reaching one just before the shoulder corner. Near to the shoulder portion, flow expansion fan is clearly visible. A large recirculation bubble is formed at end of base as shown in Fig.4.5 and also shear layer enclosing the separation bubble coalesces at the neck from where recompression shock is formed.

Normalized pressure contours for Mach 8 and Mach10 conditions are shown in Figs.4.6 and 4.7 respectively. Maximum pressure generates in bow shock around 80 times of free stream pressure for Mach 8 conditions and corresponding high pressure value in Mach 10 condition is 130 times of the free stream condition.

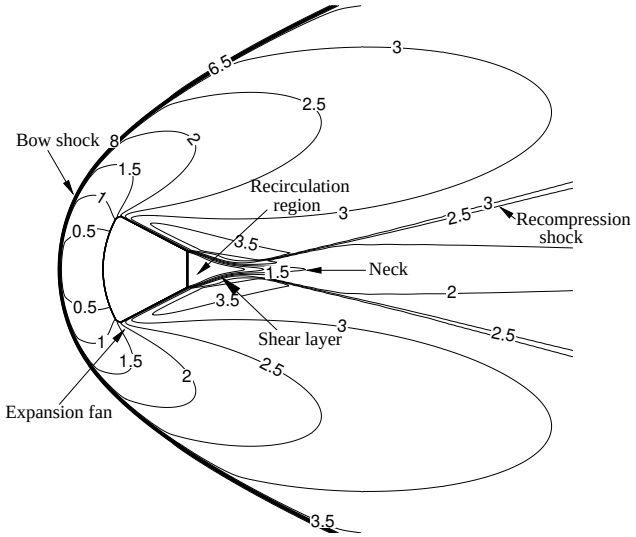

Figure 4.5: Mach contours at an altitude of 15 km for Mach 8 with 0^o angle of attack

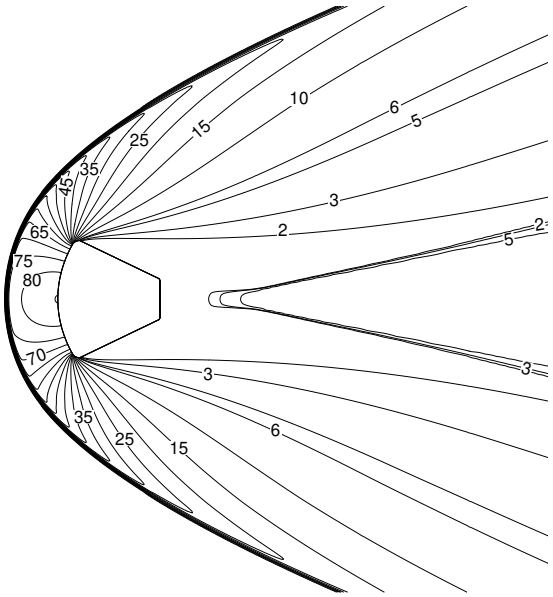

Figure 4.6: pressure contours at an altitude of 15 km for Mach 8 with 0^o angle of attack

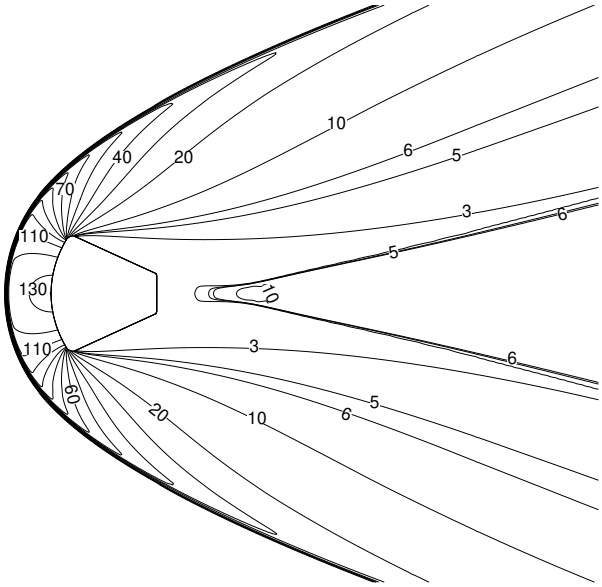

Figure 4.7: Pressure contours at an altitude of 15 km for Mach 10 with 0^o angle of attack

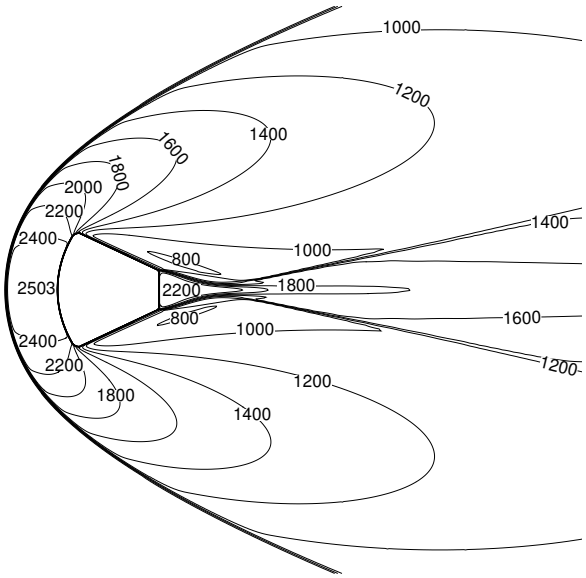

Figure 4.8: Temperature contours at an altitude of 15 km for Mach 8 with 0^o angle of attack

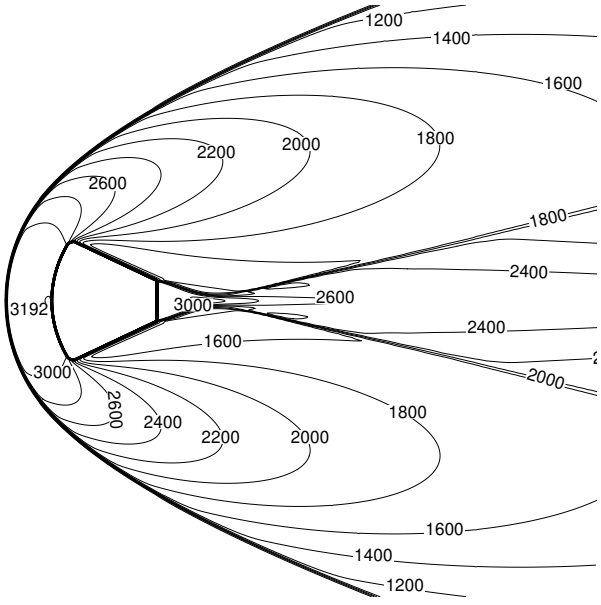

Figure 4.9: Temperature contours at an altitude of 15 km for Mach 10 with 0^o angle of attack

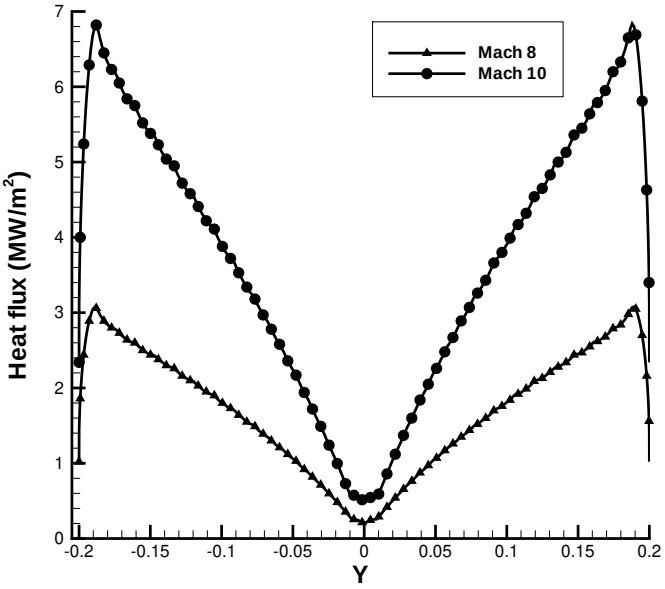

Figure 4.10: Heat flux compression for Mach 8 and Mach 10 condition at altitude 15 Km for 0^o angle of attack

Temperatures contours corresponding to Mach 8 and Mach 10 conditions are shown in Figs.4.8 and 4.9. Maximum temperature in bow shock zone is 2503 K for Mach 8 and 3192 K for Mach 10 near to center of the nose radius. Maximum temperature zone is attached to fore body of re-entry vehicle. It is complete opposite nature as shown in rarefied region that maximum temperature generated away from the surface of nose radius. High temperature also generates in the recirculation zone due to turbulent heating. Maximum temperature in the recirculation region is around 2200 K for Mach 8 and 3000 K for Mach 10 condition.

Comparison of Heat flux distribution over the fore body of the re-entry vehicle corresponding to Mach 8 and Mach 10 conditions is shown in Fig.4.10. It is observed that stagnation condition at the nose radius which corresponds to maximum temperature and minimum heat transfer rate. Maximum heat flux generates at the shoulder portion of the fore body due to thinning of the boundary layer and it is followed decrease in heat flux from the shoulder due to expansion fan. Maximum heat flux observed 3.06 MW/m^2 for Mach 8 and corresponding for Mach 10 is 6.82 MW/m^2.

4.3.2 Effect of altitude

To know the effect of altitude on thermal load, results are obtained at an altitude of 15 km and 20 km with zero angle of attack for Mach 8 conditions. Comparison of Heat flux

variation over nose radius of re-entry vehicle is shown in Fig.4.11. It is observed trend of heat flux for both altitude remain same maximum at shoulder corner and minimum at nose center. At 15 km altitude heat generation is higher compare to the 20 km altitude due to increase in density leads to more friction. Maximum heat flux observed 3.06 MW/m^2 for 15 km altitude while maximum value heat flux for 20 km altitude is 0.98 MW/m^2 .

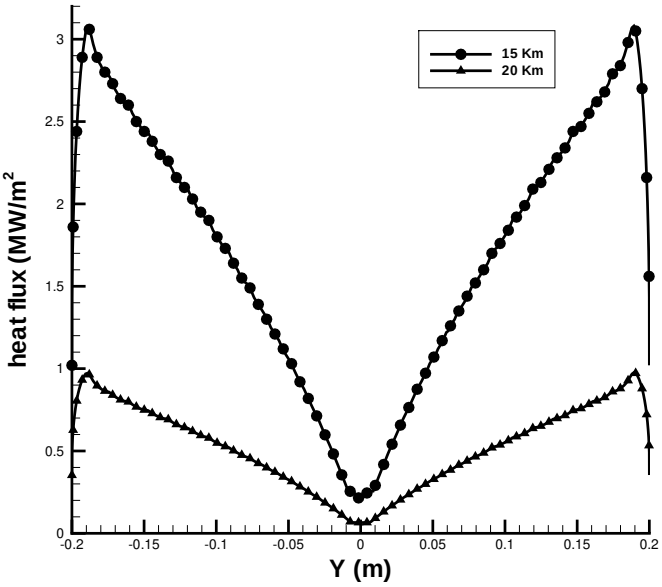

Figure 4.11: Heat flux compression for different altitude at Mach 8 for 0^o angle of attack

Chapter 5

Conclusions

Aerothermodynics analysis of NASA's Orion crew exploration vehicle (CEV) re-entry vehicle investigated numerically in rarefied region at high altitude and high density at low altitude of the earth. Different computation tools used to evaluate aerothermal load in the non-continuum rarefied field and continuum high density region.

Direct simulation Monte Carlo method is used for simulation in rarefied field regime. Tuning of DSMC method for rarefied analysis has been conducted by comparing results with standard hollow cylinder flare case. Flow field characteristics at different altitudes in the rarefied regime are reported for ideal gas and real gas model at altitudes in range of 90 km to 125 km. Real air modeled as made of five spices with 17 reacting reactions to take care of dissociation , recombination and ionization effect at the high temperature. The surface heat flux is 33.67% higher in ideal gas model compared to real gas model at an altitude of 100 km. The peak heat flux increases with decrease in altitude due to increase in density of air. The bow shock strength is doubled with an increase in free stream velocity from 7.5 km/s to 11 km/s. Aerodynamic heating of re-entry vehicle increases with increase in free stream velocity due to increase in strength of bow shock in front of vehicle. The peak heat flux at stagnation point decease with increase in nose radius. Effect of free stream velocity at low altitude is studied here. Maximum heat flux increases with increase in Mach number due increase of shock strength. At low altitude maximum temperature region is very close to the surface of vehicle compared to rarefied regime. Present results of both high and low density regime would be useful for design of thermal protection system of Orion CEV re-entry vehicle.

Chapter 6

Scope of future work

As this was the beginning of towards the study of Orion CEV re-entry vehicle at different altitudes of the earth. It is restricted to below 40 Km altitude in high density region and above 90 Km altitude in rarefied field. This work can be further expanded to altitude range between 40 km to 90 km altitude of the earth. Above 30 km altitude, the vehicle speed is greater than Mach 10. Due to this higher speed it leads to generations of very high temperature and non-equilibrium flow around re-entry vehicle. Specific heat relations with temperature available only up to 4000 K. Above these temperature modified specific heat relations based on theoretical hypothetical can be used. To take dissociations, recombination and ionizations effect at high temperature in continuum flow regime five species chemical kinematics model would be required to include. In the transition zone, at altitude 75 km to 90 km coupling of the continuum and non-continuum rarefied zone can be done by using the Bridging formulas.

Procedure used in this work for Orion CEV re-entry vehicle can be further used to study of other re-entry vehicles and also ballistic missiles. Present results of both high and low density regime would be useful for design of thermal protection system (TPC) of Orion CEV re-entry vehicle. Generally TPC to re-entry vehicle at high temperature and high heat flux is provided in terms of ablative material coating. An ablation code can be developed to predicate optimize thickness of the ablative material for safety of re-entry vehicle against high thermal load.

References

[1] Geogory P. Kennedy. *Vegeance Weapon 2: The V-2 Guided missile. Smithsonian Insition press 1983.*

[2] Dennis R.Jenkins, Tory Landies and Jay Miller. *American X-Vehicles: An Inventory X-1 to X-50. June 2003.*

[3] L Robert,O Neal and Leonard Rabb. *Heat shield performance during atmospheric Entry of project mercury Research and Development Vhicle NASA. May 1961.*

[4] Barton C.Hacker and James M. Grimwood. *On the shoulders of Titans: A History of project Gemini.NASA SP-4206, 1977.*

[5] Robert O. Pillar and Caldwell J. Johnson. *Johnson Apollo spacecraft Design. , NASA Industry Apollo Technical Conference : A Compilation of the papers presented July 1961;18-20.*

[6] Anon. *NASA's exploration systems architecture study, final report. NASA TM-2005-214062, November 2005.*

[7] H.J.Allen . *Hypersonic Flight and the Reentry Problem.Journal of the Aeronautical Sciences, 1958;25: 217-230.*

[8] A.J.Eggers *Performance of Long Range Hyper velocity Vehicles.Jet Propulsion, 1958; 27: 1147-1151.*

[9] T. A. Heppenheimer. *Facing the Heat Barrier: A History of Hypersonics. The NASA History Series , September 2007.*

[10] Moretti G. and M.Abbett. *A Time-Dependent Computational Method for Blunt Body Flows AIAA J. December 1966;4(12):2136-2141.*

[11] John J. Bertin and Russell M. Cummings. *Fifty years of hypersonic: where weve been, where were going. Journal of Progress in Aerospace Sciences 2003; 39: 511-536.*

[12] Brian R.Hollis and Salvatore Borrelli. *Aerothermodynamics of blunt body entry vehicles. Journal of Progress in Aerospace Sciences 2012;48-49:42-56.*

[13] A. Viviani, G. Pezzella. *Computational flow field analysis over a blunt-body re-entry vehicle. Journal of Spacecraft and Rockets 2010; 47 (2): 258-270.*

[14] Giuseppe Pezzella. *Aerodynamic and aerothermodynamic trade-off analysis of a small hypersonic flying test bed .Journal of Acta Astronautica 2011; 69:209-222.*

[15] Fulvio Stella,Marilena Giangi,Fabio Paglia,Marco Dascenzi and Marco Iannuccelli. *Numerical Simulation of Re-Entry Flow: Heat Flux Evaluation. Journal Heat transfer Engineering,Taylor and Francis 2006;27(2):58-69.*

[16] Giuseppe Pezzella. *Hypersonic environment assessment of the CIRA FTB-X re-entry vehicle. Journal of Aerospace Science and Technology March 2013; 25(1): 190-202.*

[17] Kunihiko Ohtake. *Thermal analysis of the thermal protection system for the re-entry vehicle. Computers methods in applied mechanics and science 1998; 151:301-310.*

[18] Raffaele Savino ,Mario De Stefano Fumo ,Diego Paterna and Michelangelo Serpico. *Aerothermodynamics study of UHTC-based thermal protection systems. Journal of Aerospace science and Technology 2005;9:151-160.*

[19] G.A.Bird . *Molecular gas dynamics and the direct simulation of gas flows. Oxford 1994.*

[20] N.Bellomo, P.Letallec and B. Perthame. *The solution of the nonlinear Boltzmann Equation:A Survey of Analytic and Computational Methods. Computers methods in applied mechanics and science 1995;30(7):21-30.*

[21] Saric WS, Muylaert J and Dujarric C. *Hypersonic experimental and computational capability, improvement and validation. AGARD AR-319 May 1966; vol. I.*

[22] R. L. Kruse. *Transition and flow reattachment behind an Apollo like body at Mach numbers to 9. NASA TN D-4645,1968.*

[23] B. R. Hollis , K. T. Berger,T. J.Horvath ,J. J.Coblish ,J. D.Norris ,R. P.Lillard ,etal. *Aeroheating testing and predictions for project Orion Crew Exploration. Journal of Spacecraft and Rockets 2009;46(4):76680.*

[24] K.Sinha and D. K. Reddy *Hypersonic turbulent flow simulation of FIRE II re-entry vehicle afterbody. Journal of Spacecraft and Rockets 2009,46(4):2009.*

[25] Muylaert J, Kumar A and Dujarric C. *Hypersonic experimental and computational capability, improvement and validation. AGARD AR-319 May 1998; vol. II.*

[26] Raffaele Votta, Antonio Schettino and Aldo Bonfiglioli. *Hypersonic high altitude aerothermodynamics of a space re-entry vehicle. Journal of Aerospace science and Technology March 2013;25(1):190-202.*

[27] John D.Anderson *Hypersonic and High -Temperature Gas dynamics. 2nd edition. AIAA Education series 2006.*

[28] W.G. Vincenti and C.H. Kruger. *Introduction to Physical Gas Dynamics. Wiley New York, 1965.*

[29] G.J. LeBeau. *A parallel implementation of the direct simulation Monte Carlo. Computer Methods Applied Mechanical Engineering 1999; 174:319-337.*

[30] C. Park, S.H. Lee. *Validation of multi-temperature nozzle flow code NOZNT .Journal of Thermodynamics and Heat Transfer 1995;9(1):9-16.*

[31] Domenic D Ambrosio . *A study on Shock Wave Boundary layer Intrection in High-Speed Flows.* 4^{th} *Europ Symp. Aerothermodynamics for Space Applications, Capula ,Italy. ESA Sp-48 2002;733-741.*

[32] US Standard atmosphere 1976. *National oceanic And Atmospheric Administration,National Aeronautical and Space Administration and US Air Force 1976.*